DISTRIBUTION OF DEMERSAL FISHES ON UNCONSOLIDATED BOTTOM HABITAT OF THE NORTHERN GULF OF MEXICO

A Thesis

by

JASON WILLIAM MOSTOWY

Submitted to the Office of Graduate and Professional Studies of
Texas A&M University
in partial fulfillment of the requirements for the degree of

MASTER OF SCIENCE

Chair of Committee,	Jay Rooker
Committee Members,	Robert David Wells
	Hiu Liu
Intercollegiate Faculty Chair,	Anja Schulze

August 2020

Major Subject: Marine Biology

ABSTRACT

Benthic habitat on the continental shelf in the northern Gulf of Mexico (NGoM) is dominated by large plains of unconsolidated terrigenous sediment. This unconsolidated bottom habitat (UBH) is presumed to be sparsely inhabited by demersal fishes, and little is known about the factors that structure the distribution and abundance of fishes on UBH. In this study, an integrated acoustic/video approach was employed to quantify the distribution of demersal fishes on UBH across the continental shelf off Texas. Split-beam echo sounder surveys were paired with simultaneous video from imaging sonar and standard cameras to determine the occurrence and density of demersal fishes on UBH. The relative performances of the different gear types at detecting and enumerating both demersal fishes and bottom relief anomalies were compared. Occurrence (presence/absence) and density of demersal fishes was then related to a suite of habitat and environmental variables using generalized additive models (GAMs) to identify the variables that contribute to the quality of UBH used by demersal fishes. Standard camera video performed poorly for detection and enumeration of demersal fishes as well as bottom relief anomalies associated with UBH due to the persistent nepheloid layer at all locations surveyed. Echo sounder and imaging sonar surveys showed similar performances in detecting fishes and relief anomalies, but their performance varied in enumerating both variables. GAMs constructed from the echo sounder dataset indicated that a shallow depth, high percent coverage and large size of relief anomalies, low salinity, warmer temperature and closer proximity to non-platform artificial structure positively influenced the quality of UBH for demersal fishes. Close proximity to active petroleum platforms had a slight negative influence. The results of this study provide insight into the factors that regulate the distribution and abundance of demersal fishes in the

NGoM, and the methodological refinements developed here will guide future efforts to characterize populations of demersal fishes on UBH.

DEDICATION

To my family, for their unerring support at every sharp turn my life takes; And to my friends and fellow TAMUG graduate students, whose perseverance and good humor are a constant inspiration.

ACKNOWLEDGEMENTS

I'd like to thank the chair of my committee, Dr. Jay Rooker, for his guidance and patience during my time at Texas A&M University. I would also like to thank my committee members, Dr. R.J. David Wells and Dr. Hui Liu, for their advice and support throughout the course of this project.

The fieldwork component of this project would not have been possible without the generous assistance of Phillip Sanchez, Shane Stephens, Christopher Steffen, Dr. John Mohan, Jillian Gilmartin, Dr. Thomas TinHan, Mariah Livernois, Liam Batchelder, Kelsey Martin and Jason Williams. Special thanks are owed to Benjamin Binder, Allison White, Dr. Marta D'Alia, Kelsey Martin and Jill Thompson-Grim for their assistance in developing the acoustic data collection and processing methodologies. Thank you to Dr. Matthew Streich for his provision of geospatial data.

This research was made possible by funding from the Mississippi-Alabama Sea Grant Consortium.

CONTRIBUTORS AND FUNDING SOURCES

Contributors

This work was supervised by a thesis committee consisting of Professors Jay Rooker, R.J. David Wells and Hui Liu of the Department of Marine Biology.

All work conducted for the thesis was completed by the student independently.

Funding Sources

Graduate study was supported by a fellowship from Texas A&M University, and this research was made possible by funding from National Oceanic and Atmospheric Administration Grant NA16OAR4170181. Its contents are solely the responsibility of the author and do not necessarily represent the official views of the National Oceanic and Atmospheric Administration or the Mississippi-Alabama Sea Grant Consortium.

NOMENCLATURE

ARIS	Adaptive resolution imaging sonar
GAM	Generalized additive model
NGoM	Northern Gulf of Mexico
NSST	Narrow-scope single targets
RALP	Relief anomaly linear proportion
SSS	Sea surface salinity
SST	Sea surface temperature
TL	Total length
UBH	Unconsolidated bottom habitat

TABLE OF CONTENTS

LIST OF FIGURES

FIGURE Page

LIST OF TABLES

1. INTRODUCTION

The distribution and abundance of fishes in marine ecosystems are structured by multiple ecological drivers working on a range of spatiotemporal scales. Immediate biotic imperatives such as prey availability (McCawley et al. 2006) and predation risk (Rooker et al. 2018) often influence individual habitat use at the seascape scale. Other factors, such as physicochemical conditions (Kotwicki et al. 2005, Hazen et al. 2009), the supply of recruits (Doherty and Fowler 1994), and reproductive behaviors (e.g., spawning aggregations; Sala et al. 2001) can generate patterns in fish distributions that manifest on larger intervals of space and time. These structuring factors rarely act in isolation in marine ecosystems, and observed distributions of fishes are often the result of a variety of interacting factors (Bowler and Benton 2005, Ryer et al. 2010, Furey et al. 2013). Disentangling the relative influence of each of these factors is necessary to identify important scalars of fish habitat quality, which in turn will improve our ability to forecast, conserve, and manage demersal fish populations (Langton et al. 1996, Lloret et al. 2002).

Previous research suggests that a suite of biotic and abiotic factors govern the suitability of demersal fish habitats in the northern Gulf of Mexico (NGoM). Physicochemical and hydrographic conditions are known to influence the distribution, abundance, and structure of demersal fish assemblages across the continental shelf in the NGoM (Monk et al. 2015, Plumlee et al. 2020). The inner shelf of the NGoM coincides with the outflow of several large rivers, most notably the Mississippi/Atchafalaya River System (MARS) (Walker et al. 2005), while the outer shelf is dominated by oceanic water associated with mesoscale oceanographic features such as the Loop Current and accompanying eddies (Lugo-Fernandez 1998). Inner shelf habitats in the region are often characterized by high primary productivity, lower and variable surface salinity, seasonal temperature variability, and high turbidity throughout the water column (Li et al. 1997,

Lohrenz et al. 1997, Lohrenz et al. 1999, Chen et al. 2000). Near the MARS delta, increased nutrient input during the spring results in seasonal hypoxic conditions across large portions of the seabed of Louisiana and Texas (Rabalais et al. 2002), which is known to affect the spatial distribution and survival of demersal fishes (Hazen et al. 2009, Craig 2012). The magnitude of freshwater discharge by MARS may generate a seasonal cross-shelf salinity gradient with areas closer to MARS showing estuarine character, and Monk et al. (2015) found that species assemblages nearest the river outflow were distinct from all other Texas/Louisiana zones examined. In contrast to inshore habitats, outer shelf areas experience oceanic conditions (Rezak et al. 1990), and the persistence of a relatively stable environment has permitted the development of complex benthic biogenic structure, including hermatypic coral reefs (Schmahl et al. 2008). Prior studies have associated this habitat gradient with shifts in fish assemblage composition from inner to outer shelf, and salient cross-shelf changes in community structure have been reported previously for fishes inhabiting both natural banks and artificial reefs (Chittenden and MacEachran 1976, Gallaway et al. 1981, Ajemian et al. 2015).

One of the most influential factors that affects the distribution of demersal fishes in the NGoM (particularly for reef-dependent fishes) is the presence of hard substrate or vertical relief of the seabed (Dennis and Bright 1988), and the presence and complexity of artificial reefs (Ajemian et al. 2015, Plumlee et al. 2020). Available hard bottom habitat on the continental shelf of the NGoM is limited, with natural banks covering approximately 2% (1600 km^2) and artificial reefs less than 0.1% (20 km^2) (Parker et al. 1983, Gallaway et al. 2009). The remainder of the bottom habitat in this region is largely composed of plains of loose terrigenous sediments. This unconsolidated bottom habitat (UBH) typically supports considerably lower fish biomass relative to more complex natural and artificial relief structures (Stanley and Wilson 1997, Boswell et al.

2010). Despite their low fish densities, UBH play a critical role in the ecology of demersal fishes on the NGoM inner shelf, supporting robust communities of small-bodied invertebrates and fishes which serve as low-level consumers in regional food webs (Wells et al. 2008a, Monk et al. 2015). Structure-associated consumers may leave complex habitats at night to forage on UBH (Gallaway et al. 1981, Peabody and Wilson 2006), while larger mobile predators may dissociate from structure altogether and inhabit UBH almost exclusively (Gallaway et al. 2009). Areas of UBH with some low bottom relief or unconsolidated structure such as shell rubble can serve as important nursery habitats for juvenile reef-associated fishes (Rooker et al. 2004, Patterson et al. 2005, Wells et al. 2008b). Modest bottom relief features in these habitats are often associated with increased biodiversity and fish abundance (Thrush et al. 2001, Thrush et al. 2002, Hewitt et al. 2005).

Characterizing the distribution and abundance of demersal fishes on UBH is complicated by the methodological restrictions imposed by typical conditions associated with this habitat. Commonly used sampling methodologies such as visual surveys, trawl surveys, and hydroacoustics each possess their own limitations that may bias abundance estimates because the performance and efficiency of these methods vary as functions of seabed complexity and water column visibility. Visual surveys conducted with SCUBA or cameras on remotely operated vehicles (ROV) are only occasionally useful on soft-bottom habitats in the NGoM because visibility is often limited by a persistent nepheloid layer (Gallaway et al. 1981, Rezak et al. 1990). Bottom trawls can be used to quantify and identify demersal fishes, but the capture efficiency of this gear is affected by size and species (Wells et al. 2009), and does not perform well when bottom complexity or relief anomalies are encountered (Zimmerman 2003). Hydroacoustic surveys are capable of providing high-resolution information on fish abundance

across a variety of benthic habitat types, and echo sounders have been successfully used to quantify the relative abundance of fishes on natural (Wilson et al. 2003, Stanley et al. 2006) and artificial (Boswell et al. 2010) reefs in the NGoM. However, definitive species identification is generally unattainable from narrow-band acoustic backscatter alone (Horne 2000, Parker-Stetter et al. 2009), and thus assemblage composition obtained from visual surveys or bottom trawls is often used in conjunction with echo sounder data to apportion taxon-specific estimates of abundance (reviewed by McClatchie et al. 2000). New approaches such as imaging sonars which produce near-video quality images of acoustic targets are increasingly used to overcome identification problems in no or low visibility conditions, and integrated surveys that couple these methods show considerable promise for estimating fish abundance across multiple habitats and/or environmental conditions (Holmes et al. 2006, Mueller et al. 2010, Langkau et al. 2012, Able et al. 2014).

The purpose of this study was to determine the abundance and distribution of demersal fishes on UBH across the continental shelf off Texas in the NGoM using an integrated acoustic/video approach. Standard echo sounder surveys were used to estimate demersal fish occurrence and density within the survey areas. Concurrent imaging sonar and standard camera videos were collected with the acoustic data. The relative performances of each gear type at detecting and enumerating fishes and bottom relief anomalies were compared. Generalized additive models (GAMs) were then employed to determine the habitat characteristics and environmental conditions associated with the probability of fish presence and elevated fish density on UBH. The two main objectives of the study were evaluated under the framework of the following null and alternative hypotheses:

Hypotheses: Gear Performance Comparison

H_{0_1}: All 3 gear types will perform equally effectively at detecting and enumerating demersal fishes and bottom relief anomalies

H_{A_1}: Gear types will vary in their effectiveness at detecting/enumerating demersal fishes and bottom relief anomalies

Hypotheses: Occurrence and Density of Demersal Fishes

H_{0_2}: Occurrence (presence/absence) and density of fishes will not be influenced by spatiotemporal factors or environmental conditions

H_{A_2}: Variation in the occurrence and density of fishes will be attributable to spatiotemporal factors and environmental conditions

2. METHODS

Study Area

Integrated echo sounder, imaging sonar, and standard camera video surveys were conducted in 2018 and 2019 across the continental shelf off Texas in the NGoM. The survey area was bounded between 26.0-29.3°N and 97.3-93.5°E, and surveys targeted shelf areas with no known bathymetric features or relief. The majority of surveys were performed in the summer and fall, during daylight hours or immediately before dawn/after dusk.

Data Collection

Echo Sounder Survey

Echo sounder transects were conducted at 147 sites off Texas in the NGoM (Fig. 1) using a SIMRAD EK80 WBT transceiver operating a single split-beam 70 kHz ES70-18CD transducer. During echo sounder transects, the transducer was either mounted directly to the side of the vessel or deployed on a custom tow body (Fig. 2). The system was calibrated prior to deployment using a tungsten carbide sphere with a nominal target strength (TS) of -40.56 dB. The transceiver was operated at the narrow-band 70 kHz setting, at the maximum pulse rate permitted by the depth with a pulse duration of 0.256 ms.

Echo sounder transects were conducted at a vessel speed of 2-4 kts for 20-30 minutes. Headings were selected randomly when possible, but conditions often necessitated maintaining a heading into the direction of the prevailing swell. Acoustic data were georeferenced at collection time using NMEA GPS string feeds from either a handheld GPS (small vessel) or the shipboard NMEA feed (large vessel). Linear distance of echo sounder transects combined was 308.8 km.

Imaging Sonar and Standard Camera Video Surveys

ARIS (Adaptive Resolution Imaging Sonar) imaging sonar and standard camera video surveys were conducted simultaneously during echo sounder surveys at transect stations where conditions and vessel capabilities permitted the deployment of video collection gear (n = 44). Both gears were mounted on a second tow body (Fig. 3). The imaging sonar unit (ARIS Explorer 1800 model) was mounted in the center of this tow body, with the sonar oriented perpendicular to the plane of the seafloor. One GoPro camera (Hero 6 Black model) was mounted directly on top of the imaging sonar unit, facing downward in the same direction as the sonar swath. A second GoPro camera was mounted at the front of the tow body, facing forward (i.e., in the direction of motion). The imaging sonar was not deployed at some sites in summer 2018- during this year, two forward-facing GoPros were mounted on a third tow body (Fig 4).

The video collection tow body was towed at a range of 4-15m from the bottom. The imaging sonar was permitted to automatically adjust its operating frequency based on the range to the bottom, switching between the 1.8 MHz identification frequency at close range and the 1.1 MHz detection frequency at longer range.

Data Processing

Acoustic Data Processing

Acoustic data from the echo sounder were processed using standard echo counting and echo integration methods (Rudstam et al. 2012). All acoustic data processing was performed in Echoview 10 (Echoview, LLC). Echograms were first visually inspected for quality to remove echograms showing excessive transducer movement or ping dropout due to surface noise

(Parker-Stetter et al. 2009). Remaining echograms were first preprocessed to remove noise and identify a bottom line. The bottom (seabed) appears on echograms as a conspicuously strong echo; the bottom line delineates the uppermost boundary of this echo and serves as a lower bound for subsequent analyses. The bottom line was identified from the S_v (volume backscatter) data using Echoview's best bottom candidate algorithm. The bottom line was manually edited to span gaps and then raised by 0.25 m to ensure that subsequent analyses were not contaminated by strong seabed echoes. Electrical impulse noise was filtered from the echogram and surface noise was eliminated by excluding data above 5 m range. Echograms were then visually inspected and large regions of non-fish backscatter were removed manually.

The total number of targets within an echogram was determined by combining the abundance attributable to individual single targets (echo counting) with that attributable to school targets (echo integration). First, schools were detected from the cleaned S_v echograms using the SHAPES algorithm (Coetzee 2000) with a minimum data threshold of -60 dB (Parker-Stetter et al. 2009). Schools were manually edited to remove areas where the algorithm had incorporated single fish tracks into a school body.

Non-school fish density was the determined through a cone model echo counting method (Kieser and Mulligan 1984). School regions were excluded from the echogram, and single targets outside of schools were detected using the split-beam single target detection algorithm of Soule (1997). As most of the echograms were empty save for a small number of fish tracks, single target detection parameters were widened from their defaults to ensure that marginal targets were included in the analysis. The TS (target strength) threshold was set to -75 dB, the normalized pulse length bounds were 0.5 - 2 lengths, the maximum beam compensation was 9 dB, and the maximum major and minor axis deviations were 0.6 standard deviations. A higher

maximum beam compensation can introduce upward bias into the final counts, but the work of Parker-Stetter et al. (2009) suggests that increasing the maximum beam compensation to 9 dB likely introduces only a small bias. After target detection, single target echograms were divided by a 90m horizontal x 20m vertical cell grid. Single target echo density within a cell was calculated by dividing the cell single target count by the cell beam volume sum.

School fish density was determined by scaling the in-school S_v by the TS (target strength) of single targets in close proximity to the school. This was performed under the simplifying assumption that the fish closely associated with a school would have a comparable TS distribution to the fish within the school body and thus could serve as an approximate *in situ* estimate of mean school TS (MacLennan and Menz 1996). First, a buffer zone of approximately 5 m was drawn around each school to encompass TS measurements from nearby single targets. The single target detection algorithm was applied to the TS within this school buffer. This pass of the single target detection algorithm employed narrower parameters than the algorithm for the single targets described above. Maximum beam compensation was set to 6 dB, normalized pulse length bounds were 0.75 - 1.5 lengths, and the maximum major and minor axis deviation remained at 0.6 standard deviations; hereafter these single targets will be referred to as narrow-scope single targets (NSST).

NSST identified within the school buffer region were filtered using the Sawada index (N_v, Eq. 1) and the ratio of multiple echoes ($M_{\%}$, Eq. 2) to ensure that single targets used to scale the in-school S_v values were not contaminated by echoes from multiple targets (Sawada et al. 1993). NSST were first binned into small cells (5m horizontal x 5m vertical) and N_v and $M_{\%}$ were calculated for each cell. Cells where $N_v < 0.1$ and $M_{\%} < 100$ were considered to contain

NSST which were sufficiently isolated to be used to scale the in-school S_v values of nearby schools.

Eq 1) $N_v = \frac{c \cdot \tau \cdot \psi \cdot r^2 \cdot n}{2}$

where c is the speed of sound in water (m/s), τ is the pulse duration (s), ψ is the equivalent beam angle (steradians), r is the range (m), and n is the density of targets as determined by S_v scaling.

Eq. 2) $M_{\%} = \frac{n - n_s}{n}$

where n is the density of targets as determined by S_v scaling and n_s is the density of targets as determined by echo counting.

To scale in-school S_v values, a school mean TS value was first calculated by averaging the backscattering cross-sections ($\sigma_{bs} = 10^{TS/10}$) of all NSST within 5m of the school border. The school S_v echogram was then divided into a 90m horizontal x 20m vertical grid, and the density of single fish targets within the school was calculated according to Eq. 3

Eq. 3) $\rho = \frac{s_v}{\sigma_{bs\_\mu}}$

where ρ is the volume density of fish targets (ind.$\cdot m^{-3}$), s_v is the linear volume backscattering coefficient and σ_{bs_μ} is the average backscattering cross-section of the NSST associated with that school. The total density of fish within a cell was calculated by a cell-wise summation of the density of school-associated targets with the density of single targets. A cell fish abundance was

also calculated by multiplying the cell fish density by the cell volume. Cells at depths >20m from the bottom were omitted from further analyses, as the focus of this study was demersal fishes.

Relief anomalies (patches of habitat where relief height diverged from the surrounding flat bottom) were identified from echograms by visual inspection using two criteria: 1) a visible height divergence from the surrounding bottom in the echogram; and 2) a discontinuity in bottom echo strength. Once located, the length and height of each relief anomaly feature was approximated by drawing a bounding box around the feature.

Imaging Sonar Video Processing

Imaging sonar recordings from the ARIS were examined for the presence of fish and relief anomalies within a transect. Fish targets were enumerated and their size along their largest presented aspect was estimated using the measurement tool in Echoview. Fish targets were classified into one of four size targets (Fig. 5): micro (too small to measure individual targets); small (5-20cm total length [TL]); medium (20-50cm TL); and large (>50cm TL). Distinguishing individual fish targets in compact schools was often difficult and, in these cases, the number of fish in the school was estimated based on the dimensions of the school and the size of targets within the school was estimated from targets at the school margins. Relief anomalies were identified by disruptions in the shape of the bottom echo. As the dimensions of these disruptions were difficult to measure accurately, relief anomaly size was classified by the duration a feature remained in the sonar swath and by a qualitative estimate of its size (Small, Medium, Large) compared with other relief anomalies (Fig. 6).

Standard Camera Data Processing

Fish appearing in the standard camera videos were counted and identified to the lowest possible taxonomic level. Species or genus designations were only assigned if a positive identification could be made (Fig. 7). Fish were dispersed enough within videos for each individual to be counted. Fish which were seen to follow or track the tow body were only counted on their first appearance in the frame.

Habitat Models

Models of the demersal fish distribution on UBH were constructed from both occurrence (presence) and density data generated by the echo sounder because this gear was used at all stations and thus had the widest spatial coverage. Generalized additive models (GAMs) were selected to model associations between demersal fish density and habitat variables. GAMs are an extension of the generalized linear model that can approximate relationships between explanatory and response variables as complexity-penalized smooth functions (Hastie and Tibshirani 1987). The general formula for a GAM is as follows:

$$\mu = g^{-1}(\beta_0 + s(x_1) + \ldots + s(x_i))$$

where μ is the expected value of the response variable, β_0 is the intercept, $s(x_i)$ is a smooth function of covariate x_i, and g is a link function which maps the linear predictor to the response variable. All GAMs were constructed using the mgcv package in R (Wood 2019, R Core Team).

The distribution of demersal fishes on UBH was modeled in two steps following Barry and Welsh (2002). In the first, the presence of fish in a 90m horizontal x 20m vertical grid cell

was modeled as a binomially distributed response probability with a logit link function. In the second, log-transformed fish density in cells where fish targets were detected was modeled as a Gaussian-distributed variable with an identity link function.

The set of potential explanatory variables was generated from a variety of sources (Table 1). Sea surface temperature data were obtained from NOAA's L4 Nighttime Global High-Resolution Sea Surface Temperature product at 5km resolution (https://coastwatch.noaa.gov/cw/satellite-data-products/sea-surface-temperature). Sea surface salinity data were obtained from HYCOM's GOFS 3.1 1/12° Analysis (GLBv0.08, exp. 93.0). Chlorophyll-a concentration data were obtained from NOAA's MSL 12 L4 Ocean Color product at 9km resolution (https://coastwatch.noaa.gov/cw/satellite-data-products/ocean-color). Bottom rock composition was obtained from USGS's usSEABED dataset; the rock composition percentage field in this dataset was kriged into a rock composition percentage surface, from which a cell rock composition value was extracted (Buczkowski et al. 2020). Mean transect depth was extracted from the GEODAS US Coastal Relief model (https://www.ngdc.noaa.gov/mgg/coastal/crm.html). Locations of natural hard bottom habitats were provided by M. Streich of the Harte Research Institute's Fisheries and Ocean Health Lab (M. Streich, pers. comm.). Locations of active petroleum platforms and pipelines were obtained from the Bureau of Ocean Energy Management (https://data.boem.gov). Locations of wrecks were obtained from NOAA's Office of Coastal survey (https://nauticalcharts.noaa.gov/data/wrecks-and-obstructions.html). Locations of artificial structures were obtained from the Texas Parks and Wildlife Department (https://tpwd.texas.gov/gis/ris/artificialreefs/). Wrecks and artificial reefs were combined into a single dataset, from which the "distance from artificial structure" variable was derived. All

spatial variable extraction was performed in ArcMap (ESRI). Many variables were ln(x) or ln(x+1)-transformed to improve normality (Table 1).

Characteristics of the bottom relief anomalies within a cell were also included as explanatory variables in GAM construction. Cell variables that were associated with relief anomalies were mean and maximum relief anomaly height, mean and maximum relief anomaly length, and Relief Anomaly Linear Proportion (RALP), the summed length of all relief anomaly features in the cell divided by the cell linear distance.

The number of potential explanatory variables was reduced prior to initial model fitting in a two-stage process. In the first stage, GAMs modeling the response as a function of each individual explanatory variable were constructed and their deviance explained (DE) recorded. Any variable that explaining less than 1% of the deviance (<1% DE) in the absence of any other variables was eliminated from the potential variable set. Next, collinearity between explanatory variables was assessed with a Spearman's ρ correlation matrix. Variables that were correlated at $|\rho| > 0.6$ were incorporated into single-variable GAMs and their AIC values (Akaike Information Criterion, Akaike 1974) were compared. The explanatory variable that generated the model with the lowest AIC was included in the model selection process.

Model selection was conducted via an exhaustive search process using the Multi-Model Inference package in R (Barton 2020). As the full dataset had several thousand cells and adjacent cells were not necessarily spatially independent from one another, GAM selection was not performed on the full dataset but rather on random data subsets consisting of a group of cells whose centroids were spaced at least 1000m apart from one another (Wood et al. 2015). Once a random subset was selected, the distribution of the subset response variable was compared to the response variable distribution of the full dataset using a Chi-square (X^2) goodness-of-fit test. The

random subset was discarded if the probability of the goodness-of-fit test was < 0.1. This process was repeated until 10 different data subsets had been generated.

For each of the 10 data subsets, GAMs containing all possible combinations of the explanatory variables were generated. Smooth functions for all variables were restricted to a maximum of 4 degrees of freedom to avoid overfitting, and an offset term consisting of the log of the volume water in each cell was included in every model. Models were ranked in order of increasing AIC, and all models within 2 AIC of the most likely model were recorded (Burnham and Anderson 2002). This process was repeated for each of the 10 data subsets. GAMs that appeared most frequently (>4 times) were selected as candidate models, and refit to the full dataset for further examination. Candidate model smooth plots were examined visually to ensure that neither the direction or magnitude of the smooth terms changed significantly after refitting from the data subset to the full dataset. Final binomial and Gaussian models were selected from the candidates based on three criteria (Zuur et al. 2009): 1) parsimony, with models containing fewer terms being preferred over a model with more terms; 2) ecological explicability, with all variable effects having some straightforward ecological interpretation; and 3) performance validation, the method for which varied between the binomial and Gaussian models.

Model Validation

Candidate binomial models were validated using a repeated 5-fold cross validation method (Molinaro et al. 2005). The dataset was randomly split into 5 equally sized subsets, each containing a similar proportion of fish presence as the original dataset. Candidate models were refit on 80% of the subset and the resulting model used to predict fish presence/absence at the remaining 20% of the data. AUC or area under the ROC (receiver operating characteristic) curve

was used as measures of model performance and calculated using the ROCR package (Sing et al. 2005). Model refitting and AUC calculation was repeated for each of the 5 folds generated by the randomized data splitting. The randomized splitting process was then repeated 10 times to generate a total of 50 estimates of AUC for each model. AUCs of the candidate models were evaluated according to the performance criteria of Hosmer and Lemeshow (2000), where AUC 0.7 to 0.8 is acceptable, 0.8 to 0.9 is good, and 0.9 to 1 is excellent.

Candidate Gaussian GAMs were validated using a leave-one-out mean squared error of prediction (LOO-MSEP) minimization method (Mevik and Cederkvist 2004). A single observation was omitted from the dataset and the candidate GAM was refit to the remaining data. The refit GAM was then used to predict the response density of the omitted observation. The error of the resulting prediction was calculated and retained. This process was repeated for each observation in the dataset. The mean of the squared prediction errors was then calculated. This LOO-MSEP provided a framework for comparing the prediction performance of candidate models when presented with new data, with lower LOO-MSEP values being preferred.

Model Visualization

Once final binomial and Gaussian GAMs were selected, the influences of the explanatory variables on the responses were visualized over a grid of points with 0.0125° x 0.0125° spacing. Point grid values for most explanatory variables were obtained from the same data sources used in the model dataset. In the case of relief anomaly variables, point grid values were instead randomly generated from the dataset by drawing values of the required relief anomaly variable from that variable's empirical distribution in the cell dataset. Final GAMs were then applied to the point grid dataset to generate response predictions for each point in the grid. To account for

the effects of including randomly drawn data in the point grids, this generation-prediction process was repeated 500 times for both the binomial and Gaussian models. The final visualizations show the pointwise mean of the 500 point grid predictions. A prediction of overall UBH demersal fish habitat quality was generated by pointwise multiplication of the binomial and Gaussian point grid predictions. The habitat quality prediction was standardized to a 0-1 range, where 0 denotes areas with the lowest combined values of predicted fish presence/density and 1 denotes the highest combined values. Habitat quality was then divided by quartile into four quality categories: poor (1st quarter), fair (2nd quarter), good (3rd quarter) and excellent (4th quarter). The areal coverage of each habitat quality category was then calculated for each of 5 depth zones.

3. RESULTS

Echo Sounder Survey

Echo sounder transects were conducted at 147 stations on UBH (Fig. 8) but the quality of echograms from 7 transects was too poor for analysis, and these were removed from the dataset. The remaining 140 transects were further divided into 3,323 90m x 20m cells for estimating occurrence/density at a smaller spatial scale. Demersal fish were detected in 929 cells (28.0%, Fig. 9), and in cells where fish were present, acoustically derived densities ranged from < 0.1 to 139.3 fish·1000m^{-3}; mean of 1.0 fish·1000m^{-3} (Fig. 10). Mean target strength (TS, correlates positively with fish target size) of fish targets increased linearly with depth ($R^2 = 0.27$, $p < 0.0001$, Fig. 11). Bottom relief anomalies were detected in 412 echogram cells (12.4%). A mean of 1.2 relief anomalies were detected in cells where relief was present, and ranged from 1 to 6. Mean Relief Anomaly Linear Proportion (RALP) was 12.0% for cells with bottom relief detected and ranged from 0.3% to 87.2%.

Imaging Sonar and Standard Camera Video Surveys

Concurrent imaging sonar data were collected at 44 (31.4%) of the stations on UBH, and fish targets were detected in 41 (93.2%) imaging sonar transects. Small (5-20 cm TL), medium (20-50 cm) and large (> 50 cm) fish targets were detected in 86.3%, 68.1% and 9.0% of transects, respectively. Mean per-transect counts of small, medium and large fish targets were 208.3, 21.5 and 0.2, respectively. Bottom relief anomalies were detected in 32 (78.0%) of imaging sonar transects. Small (mean duration 2.2 ± 0.05 seconds), medium (10.8 ± 0.24 s) and

large (16.0 ± 0.45 s) structures were detected in 59.0%, 38.6% and 29.5% of the imaging sonar transects, respectively.

Standard camera video data were collected at 61 (45%) of the stations on UBH. A nepheloid layer near the bottom was present during all standard camera transects, and nearly all successful detections of fishes occurred when the cameras mounted on the tow body were several meters above the bottom and above the nepheloid layer. Fish were detected on 28 (45.9%) of the camera transects, with a total of 524 individual fishes observed (Table 2). Of these, 82.6% of the individual fish were identified to family and 55.0% to species level. Six families of bony fishes (Balistidae, Carangidae, Echeneidae, Lutjanidae, Rachycentridae, and Scombridae) and one family of sharks (Carcharhinidae) were positively identified in camera transects (Table 2). The majority of fishes identified to species were red snapper (*Lutjanus campechanus*), with this species accounting for 46.0% of all fishes identified to at least the family level. Red snapper were also the most frequently detected species and observed in 18.0% of the camera transects. Other frequently observed taxa included scombrids (11.5%) and carangids (11.5%). Bottom relief anomalies of any kind were never detected in camera transects.

Gear Performance Comparison

All three gear types (echo sounder, imaging sonar, standard camera) were deployed at 40 transects. Given that fish were rarely observed in camera transects due to poor visibility, this gear type was omitted from gear performance comparisons. Thus, the gear comparison was limited to those transects where both the echo sounder and imaging sonar were deployed (n = 44). In terms of fish detection, both gears detected fishes in 42 of the of the paired transects (93% agreement) with each gear failing to detect fish in one transect (Table 3). The echogram of

the transect in which the imaging sonar failed to detect fishes contained only a single fish track, and overall echo sounder derived fish abundance was low (11^{th} percentile).

Correlation of fish target numbers between paired echo sounder and imaging sonar transects was significant although correlation was relatively low (F-test, $r = 0.25$, $p = 0.03$, Fig. 12a). To examine the influence of school target abundances on the overall enumeration comparison, echo sounder data was restricted solely to single targets (i.e. school targets were omitted) and imaging sonar fish targets were restricted to the medium and large size classes. Omitting schooling targets and small size classes resulted in a correlation between the two enumeration methods that was considerably higher (F-test, $r = 0.75$, $p < 0.001$, Fig. 12b).

Detection of relief anomalies was generally consistent between the echo sounder and imaging sonar (66% agreement), but detection of relief anomalies using the echo sounder was higher than the imaging sonar (Table 4). The height of the relief anomalies affected their detectability with both gears. All relief anomalies identified in the imaging sonar transects where the echo sounder failed to detect relief were classified as small. Relief anomaly height in transects where the imaging sonar did not detect relief anomalies was significantly lower (Welch's 2-sample t-test, $p < 0.001$, Fig. 13a) than in transects where the imaging sonar and echo sounder both detected relief anomalies, and depth in transects where the imaging sonar did not detect relief anomalies was significantly shallower (Welch's 2-sample t-test, $p = 0.025$, Fig. 13c) than transects where the imaging sonar and echo sounder both detected relief anomalies.

In relief anomaly enumeration, no correlation between echo sounder relief anomaly counts and imaging sonar relief anomaly counts was observed ($r = -0.032$, $p = 0.837$, Fig. 14a). When imaging sonar-derived relief anomalies were restricted to larger features (defined as those

having a screen duration >1 sec), agreement between the echo sounder and imaging sonar counts was much stronger ($r = 0.753$, $p < 0.001$, Fig. 14b).

Habitat Modeling

The final binomial GAM of fish presence/absence on UBH included six explanatory variables: relief anomaly linear proportion (RALP), depth, distance from artificial structure, distance from active platforms, sea surface salinity, and sea surface temperature (Table 5). Overall deviance explained (DE) by the model was 24.2% with a mean AUC of 0.722 ± 0.0003 (acceptable, per Hosmer and Lemeshow 2000). The most influential variable was depth (ΔDE = 5.7%, ΔAIC = 247.1), with fish presence decreasing with increasing depth to a minimum at approximately 50m. RALP was another influential variable (ΔDE = 5.0%, ΔAIC = 218.5) and showed a direct relationship with fish presence increasing with on UBH with higher RALP. Increasing sea surface temperature (ΔDE = 1.7%, ΔAIC = 72.8) positively influenced the probability of fish presence, while increasing the distance from an artificial structure (ΔDE = 1.1%, ΔAIC = 47.2) generally decreased the probability of fish presence. Sea surface salinity (ΔDE = 1.0%, ΔAIC = 39.7) and distance from active platforms (ΔDE = 0.4%, ΔAIC = 13.1) were the least influential variables retained in the model and had slight positive and negative effects on the probability of fish presence, respectively (Fig. 15). Variables included in the presence/absence GAM selection process that were not retained in the final model were bottom rock composition and distance to natural hard bottom habitat.

The final Gaussian GAM of demersal fish density included three explanatory variables: mean RALP length, depth, and sea surface salinity (Table 6). DE from the final density-based GAM was 65.1%, and the model LOO-MSE was 4.8% higher than that of the model with the

lowest error. Depth was the most influential variable in the density-based GAM (ΔDE = 27.8%, ΔAIC 538.9), with increasing depth having a negative effect on fish density (Fig. 16). Less influential variables were mean relief anomaly length (ΔDE = 1.3%, ΔAIC 24.0), which had a positive effect on fish density at high values, and sea surface salinity (ΔDE = 0.8%, ΔAIC 16.2), which had a negative effect on fish density. Variables included in the density GAM selection process that were not retained in the final model were bottom rock composition, distance to pipelines, distance to oil and gas platforms, distance to manmade structure and distance to natural hard bottom habitat.

The binomial GAM predicted that the probability of demersal fish presence on UBH was generally higher inshore (Fig. 17). Depth was the most influential variable in this model, and thus it is not surprising that the effect of depth on the probability of presence is the most readily apparent in the model visualization, with a strong decrease in probability of demersal fish presence from inshore to offshore areas. The positive effect of artificial structure on the response probability appears as rings of increased probability surrounding structures, while the weaker negative effect of active petroleum platforms can be seen as smaller rings of decreased probability on UBH near these structures (Fig. 17).

Of the three variables retained by the Gaussian model of demersal fish density, one variable (salinity) was temporally dependent and thus approximated in the grid visualization by the dataset mean salinity value. Mean relief anomaly length was determined empirically, and was randomly generated to create the visualization dataset. As such, the only variable which strongly influenced the Gaussian model visualization was depth, which was sourced from a region-wide dataset. Logged demersal fish density on UBH is predicted to be much higher at shallower depths (Fig. 18).

Combining the two models in the index of UBH quality resulted in a compounding of the effect of depth, with very high predicted quality on the inner shelf and lower predicted qualities for the outer shelf (Fig. 19). The effects of nearby high relief habitats are still apparent as regions of increased (artificial structure) and decreased (active platforms) predicted habitat quality; however, on the inner shelf this effect is less apparent due to the strong positive influence of shallow depth. The influence of depth is also apparent in the quartile partition of habitat quality, and 99.9% (11,588 km^2) of UBH on the inner shelf from 10-20 m depth was classified as excellent habitat (i.e. highly suitable) for demersal fishes (Table 7). There was an order of magnitude decline in percent coverage of highly suitable UBH moving into the 20-40 m depth zone, with only 7.6% of the area and less than 1,500 km^2 classified as excellent for demersal fishes. For the next three depth zones (40-60, 60-80, 800-100m), the percentage of suitable habitat (classified as good or excellent) was 0% in all three zones. UBH classified as fair continued to decline with increasing depth and comprised less than 1% of all UBH in the deepest depth zone (80-100m) (Table 7, Fig. 20).

4. CONCLUSIONS

Survey methods employed in this study revealed that demersal fishes were widely distributed on UBH off Texas in the NGoM. Echo sounder transects showed that the distribution and abundance of demersal fishes varied spatially and small-scale patchiness was driven by the presence of bottom relief anomalies, which were also relatively common on UBH. Towed imaging sonar transects provided additional high-resolution information on both the distribution and abundance of demersal fishes as well as the extent and complexity of bottom relief anomalies. Imaging sonar deployments are often fixed, with a sonar unit continuously surveying a single area (Holmes et al. 2006, Langkau et al. 2012, Giorli et al. 2018, Plumlee et al. 2020). Mobile imaging sonar surveys have been conducted in relatively calm conditions such as lakes, estuaries, and nearshore sublittoral habitats (Able et al. 2014, Becker et al. 2017, Chang et al. 2017). This study represents one of the first attempts to use mobile imaging sonar surveys to examine large areas of open shelf habitat, and the results suggest that it shows considerable promise as a complement to traditional echo sounders in quantifying fish distributions on UBH.

Echo sounder and imaging sonar performed similarly at detecting demersal fishes on a transect-by-transect basis on UBH, with these gears only failing to detect fish on transects where fish density was very sparse (imaging sonar) or where fishes were closely associated with the seabed (echo sounder). The abundances of isolated fish targets as determined by the two methods were moderately correlated, suggesting that data collected by either method may be comparable after the application of some correction factor. However, correlation between fish counts from the two gears was much higher when small imaging sonar targets and schools detected by the echo sounder were excluded, suggesting that variation in the counts of closely packed school

target is the main source of disagreement between the fish counts produced by each data type. Enumerating individual fish targets in schools from echogram data requires a variety of assumptions regarding the acoustic properties of the fish within the school (Simmonds and MacLennan 2005). Such assumptions are not required to enumerate schooling fish from imaging sonar videos, but difficulties in distinguishing single targets in schools where fish are closely associated (e.g., tightly packed bait balls) can bias counts (Keefer et al. 2017). Automated target counting algorithms have been developed for static imaging sonar deployments (Boswell et al. 2008) and for mobile deployments in calm conditions (Jing et al. 2017). The expansion of these algorithms to survey designs involving open-ocean conditions, moving backgrounds and dense fish schools would be a useful tool for future imaging sonar assessments of fishes on UBH and UBH-like habitats.

In contrast to fish targets, the detection of bottom relief anomalies differed between the echo sounder and imaging sonar (34% disagreement in paired transects). In cases where the echo sounder did not detect relief anomalies, this was likely a consequence of its wider field of view compared to the imaging sonar. To be detected in the echogram, a relief anomaly needed to be conspicuously larger than the surrounding bottom surveyed in a given ping. Because the echo sounder was towed at a consistent depth of ~4m below the surface and surveyed an approximately cone shaped volume during each ping cycle, the area of bottom sampled per ping was larger at deeper sites. Thus, relief anomalies at deeper stations needed to be more dramatic than shallower stations in order to be detected. All five transects where the echo sounder failed to detect relief were deeper than the median transect depth (44m) and all relief anomalies detected in the corresponding imaging sonar videos were classified as small, suggesting that the echo

sounder is not effective at detecting diminutive relief at long ranges (Simmonds and MacLennan 2005).

The reasons that the imaging sonar did not detect relief anomalies in paired transects where the echo sounder did identify bottom relief is not entirely clear, but may be attributed to a depth-dependent spatial mismatch between the area of bottom surveyed by the two acoustic gear types combined with the variable size of relief anomalies on UBH. Transects where the imaging sonar detected relief anomalies were significantly deeper than transects where the imaging sonar did not detect relief (Fig. 13c). As previously discussed, the echo sounder was towed at a fixed depth relative to the surface, and surveyed an athwartship (i.e. along the vessel's port-starboard axis) swath of bottom that increased with depth. In contrast, the imaging sonar was towed at a fixed depth relative to the bottom, and thus surveyed a similarly sized swath (~5-7.5 m) regardless of site depth. In addition, the echo sounder tow body was towed relatively close to the stern of the vessel, while the imaging sonar tow body required more line payout to reach the bottom and so was necessarily deployed at a further distance from the stern of the vessel, making the imaging sonar vulnerable to subsurface currents that could deflect the tow body in an athwartship direction. At deeper sites the swath surveyed by the echo sounder is relatively wide (e.g. ~25 m across at 80 m depth), and is likely to coincide with the swath surveyed by the imaging sonar regardless of any minor deflection. At shallower sites the swath surveyed by the echo sounder is much narrower (e.g. ~6 m across at 20 m depth), and the echo sounder swath is less likely to fully overlap with that of the imaging sonar in the presence of an athwartship deflection of the imaging sonar tow body. Any resulting spatial mismatch in the bottom surveyed by the two gears would be most likely to cause a disagreement in the detection of small relief anomalies, which is supported by the significant relationship between mean relief anomaly

height and imaging sonar relief anomaly detection (Fig. 13a). The spatial mismatch issue is difficult to alleviate, but it is at least possible to account for its effects through more accurate georeferencing of the imaging sonar tow body. This could be accomplished through the use of a USBL (Ultra-Short Baseline, Vickery 1998) or similar acoustic positioning system. In any case, the ability of each acoustic gear to detect relief anomalies under certain conditions where the other gear is unable to detect them demonstrates the utility of employing both gears in tandem to measure relief over open bottom areas.

While echo sounder and imaging sonar surveys show considerable promise for characterizing the distribution of demersal fishes on UBH and the complexity of relief in this habitat, data derived from standard camera video were limited in their ability to provide information on fish assemblage compositions or habitat characteristics. This was due to the consistent presence of a turbid nepheloid layer that was present in all tows and drastically reduced visibility several meters above the bottom. The nepheloid layer frequently impedes visual surveys on natural and artificial structure in the NGoM; however, the layer is generally restricted to the base of the water column at the seabed interface and often permits visual surveys of high-relief habitats that extend well above the layer (Streich et al. 2017). The thickness and persistence of the nepheloid layer varies seasonally and regionally in the NGoM (Rezak et al. 1990), and additional standard camera transects may reveal periods where near-bottom visibility over UBH increases. Despite its limitations, the standard camera video provided some useful information on the composition of the UBH fish assemblage. Red snapper was a major constituent of the UBH fish community, which is consistent with observations from other low-relief habitat in the NGoM (Wells et al. 2009, Plumlee et al. 2020). A mix of reef-associated (e.g.

lutjanids) and pelagic transient (e.g. scombrids) fishes were detected, evidence that UBH serves as important habitat for species commonly associated with both the seabed and water column.

GAMs generated from echo sounder data found underlying structure in the distribution of demersal fishes on UBH. This suggests that variability was present across this habitat in the NGoM and influenced the occurrence and density of demersal fishes. Depth emerged as an important predictor in both presence- and density-based GAMs, with inner shelf areas being associated with a higher probability of fish presence as well as higher fish densities. Nearly 11,600 km^2 of the highest quality UBH was predicted to occur in the depth zone extending from the shallowest zone surveyed (10-20m) (Table 7). The explanation for this result is likely related to both ecological and methodological considerations. Depth is generally positively associated with body size in demersal fishes (Macpherson and Duarte 1991), and the increasing trend in TS with depth observed in this study suggests a similar pattern of increasing demersal fish size with depth (Love 1977, Rudstam et al. 2012). Our results also suggest demersal fish size increasing with increasing depth on UBH in the NGoM, with larger fish preferentially inhabiting deeper regions of the shelf. Findings from a recent study by Dance and Rooker (2019) on the cross-shelf movements of red snapper on unconsolidated substrates in the NGoM indicated that preferred depth of this species increased with increasing size/age, which is in accord with modeling results reported here. In the NGoM, many reef-associated fishes move to progressively more complex structured habitats as they grow larger, while low-relief habitat serves as nursery habitats for juveniles and subadults (Rooker et al. 2004, Wells et al. 2008b). The movement of larger, older fish to both deeper and more complex habitat types from a cohort that has experienced age-specific mortality (i.e., reductions in numbers per age class) may contribute to the negative relationship between depth and fish presence and density on UBH observed in this

study. Depth was also strongly correlated with chlorophyll-a concentration ($\rho = -0.85$), and thus the significant effect of depth likely incorporates the influence of primary productivity. During the summer and early fall, increased riverine input combined with a general northeasterly flow of water form a cross-shelf gradient of primary productivity, with high nearshore productivity and lower productivity offshore (Chen et al. 2000, Martínez-López and Zavala-Hidalgo 2009). Much of the highest-quality UBH identified in this study was restricted to a narrow band inshore of the 20m isobath (Fig. 20). The location of this discontinuity in habitat quality corresponds closely to the boundaries of the inner Texas shelf productivity region identified by Salmerón-García et. al (2011), who classified this region by its high riverine input and seasonal productivity cycles. In their study of fish and biofouling assemblages on oil platforms, Gallaway and Lewbel (1982) proposed that riverine input and water turbidity were the driving mechanisms behind a divide in assemblage composition that occurred near the 30 m isobath, where an inshore coastal/estuarine assemblage transitioned to an offshore assemblage. The results of this study suggest the existence of a similar transition zone for UBH in the 20-40 m depth range on the Texas shelf, where decreases in both demersal fish presence and density were noted relative to inshore sites. While depth serves as a useful predictor for this gradient in UBH quality, it is likely that other depth-correlated variables (e.g. productivity, turbidity, estuarine character) are also important ecological drivers of this gradient. It is also important to note that the detection of small fishes decreases with increasing echo sounder survey depth due to a decrease in the signal-to-noise ratio at larger distances from the transducer face (Simmonds and MacLennan 2005). This may also explain the observed lack of small fishes at deeper sites, although such losses should be low at the relatively shallow depths sampled in this study (De Robertis and Higginbottom 2007).

Additional explanatory variables linked to the presence and/or density of demersal fishes from GAMs were the percent cover and mean horizontal length of bottom relief. Microtopographic features such as shell patches, sand waves, and depressions are known to influence the distribution and behavior of demersal fishes on UBH (Auster et al. 1995, Wells et al. 2008b, Schultz et al. 2014, Ferrari et al. 2018), and increasing coverage and mean size of bottom relief anomalies on UBH were positively associated with demersal fish presence and density, respectively. The degree to which habitat complexity influences the distribution of demersal fishes on UBH is difficult to quantify from this study, as data were collected in linear transects while relief anomalies presumably have a radial influence on the fish distribution (Schultz et al. 2012). Assuming a nominal beam width of 18°, the echo sounder transect width at the maximum survey depth of 100m would be approximately 32m. As a result, it is possible that some of the survey cells contained fish that were associated with a bottom relief feature that was outside the transect width, and vice-versa. When considered in conjunction with limitations of echo sounder and imaging sonar surveys to detect bottom relief on UBH, it is clear that increased spatial coverage of echo sounder and imaging sonar transects within grid cells is needed to identify bottom relief characteristics that represent important habitat attributes for demersal fishes. Moreover, these relief features can be ephemeral (Gallaway et al. 2009), so repeated sampling at the same location would also be an important component of any future studies.

Proximity to complex manmade structures was also predictive of habitat quality for demersal fishes. However, the effect varied depending on the type of nearby structure, with submerged non-platform artificial structures such as intentional manmade reefs and shipwrecks having a positive effect on fish presence and active oil platforms having a marginal negative effect. Moreover, the effect was apparent on a large spatial scale: a cell within 500m of a non-

platform structure was 3.6 times more likely to have fish present than a cell 10km from a structure, but a cell 10km away was still 1.6 times more likely to have fish present compared with a cell 30km from a non-platform structure. Non-platform structures in the NGoM span a wide range of sizes, materials and vertical relief, but generally have lower vertical relief and complexity compared with standing platforms and are associated with a more structure-dependent fish assemblage (Plumlee et al. 2020). The predicted increase in quality of UBH in areas surrounding non-platform artificial structures may be due to a spillover of demersal fishes from these artificial habitats to UBH (Shultz et al. 2012). In the case of active oil platforms, a negative effect was observed. Cells 5000m away from a platform were 3.3 times more likely to have fish present than cells 500m away from a platform. Since standing oil and gas platforms are often inhabited by large transient piscivores (e.g. greater amberjack, carcharhinid sharks) that often utilize the entire water column including the seabed (Dokken et al. 2000, Ajemian et al. 2015), foraging activity by these highly mobile predators may suppress fish densities on UBH in areas near these platforms (Gallaway et al. 2009).

Sea surface temperature was also associated with the predicted quality of UBH. Sampling for this study occurred from late spring through early winter, and water temperature was strongly correlated with day of year ($\rho = -0.69$); of the two, temperature had a lower AIC on its own, which led to the exclusion of day of year in the model fitting process (Table 1). Cooler waters were associated with lower habitat quality, and similar observations of lower fish biomass on UBH during winter (lower water temperature) has been previously reported (Chittenden and MacEachran 1979). Reef fishes in the NGoM reduce the size of their movements away from structured habitat during winter months (Herbig and Szedlmayer 2016, Williams-Grove and Szedlmayer 2016), which may have led to less frequent detections over UBH during periods of

lower water temperature. Two methodological considerations may also have influenced the apparent importance of water temperature. First, demersal fishes such as red snapper are known to associate more closely with the bottom during the winter (Williams-Grove and Szedlmayer 2017), which would increase the probability of their acoustic backscatter being obscured by stronger echoes from the seabed (Ona and Mitson 1996). Second, due to limitations imposed by the size of the region sampled for this survey, water temperature was confounded with sampling location to a degree. Sampling stations with the lowest sea surface temperatures (< 24°C) were concentrated in the middle of the sampling corridor off central Texas, meaning that the effect of colder temperatures was estimated from a relatively small geographic area instead of the entire sampling corridor. This raised the possibility that the apparent decreased probability of detecting fish in colder waters was due to geographic variability instead of temperature, i.e. the transects surveyed during winter months may have been poor UBH regardless of temperature. However, when the winter transects are compared with nearby transects on the central Texas shelf region, the percentage of cells with fish present was still considerably lower in winter transects (11.7%) compared with transects conducted in nearby areas during the summer (36.8%). This suggests that temperature -not geographic variation- was the driver of fish absence at colder sites. Regardless, year-round sampling on other areas of the Texas shelf would clarify the relationship between UBH quality and seasonal temperature variation.

Sea surface salinity was retained as an explanatory variable in both the presence/absence and density models, with lower salinity associated with a higher probability of fish presence and density. The NGoM displays a cross-shelf gradient in estuarine character with salinity on the inner shelf often markedly lower than the outer shelf due to freshwater inflow from MARS and other rivers (Walker et al. 2005). The inshore-offshore salinity gradient likely plays a role in

creating distinct nearshore and offshore fish assemblages in the NGoM (Gallaway and Lewbel, 1982). Ajemian et al. (2015) found that this assemblage gradient varied between structure-associated fishes on nearshore (inner shelf) habitats to a more pelagic-associated schooling fishes chub on offshore (outer shelf) sites. If similar cross-shelf assemblage shifts in species composition also occurs on UBH, then reductions in the presence and density of demersal fishes with increasing salinity may be due in part to a cross-shelf shift to more pelagic species in high salinity, offshore waters of the NGoM because pelagic taxa show less association with the bottom and thus would be less likely to be classified as demersal fishes. The effect of salinity was relatively minor in both GAMs (Tables 5 and 6), which is likely a consequence of the simultaneous inclusion of depth in the models. While depth and salinity were not correlated enough to warrant excluding either from the GAM selection process, much of the information about the fish distribution which could be explained by a cross-shelf variation in salinity was encapsulated in the variation explained by depth, leaving little residual variation for salinity to explain.

Overall, the predicted quality of UBH for demersal fishes was found to be highly variable across the shelf areas surveyed, contradicting the supposition that this habitat is of uniform and homogenous ecological utility to demersal fishes. Echo sounder and imaging sonar surveys provided complementary data that were used successfully characterize cross-shelf patterns of occurrence and density of demersal fishes on UBH, and future improvement of the synchronization of the two data types shows considerable promise for assessments of demersal fishes in large, low visibility habitats that cannot be accurately surveyed with widely used visual approaches (e.g., ROVs, camera sleds, drop cameras). Several environmental factors were found to affect the quality of UBH, particularly depth and bottom relief. Much of the shelf inshore of

the 20 m isobath was predicted to be high quality UBH with a steep decline in high-quality UBH coverage observed in the 20-40 m depth zone, suggesting that this depth zone is a transitional area for demersal fish habitat quality in the region. The apparent importance of relief anomalies in structuring the distributions of demersal fishes on UBH merits particular focus, and a comprehensive knowledge of the sizes, shapes, and complexity of relief anomalies is needed to fully understand the ecological value of these habitat features. Species composition of the assemblage beneath the nepheloid layer on UBH remains unresolved, and future applications using multi-frequency (Kang et al. 2002) or broadband surveys (Benoit-Bird and Waluk 2020) that can apportion backscatter to taxonomic groups based on multifrequency echo responses (with caveats, see Bassett et al. 2018) may shed light on the distribution and abundance of key species that make up assemblage(s) on UBH. More refined habitat models that are based on a species presence or density—rather than the entire demersal fish community—will enhance our understanding the ecological role and function of UBH on the population dynamics of associated fishes. Given the enormous areal coverage of UBH in the NGoM and the demonstrated variability in its quality for demersal fishes, the need for such an understanding is clear.

REFERENCES

Able KW, Grothues TM, Rackovan JL, Buderman FE (2014) Application of mobile dual-frequency identification sonar (DIDSON) to fish in estuarine habitats. Northeastern Naturalist 21(2): 192-210

Ajemian MJ, Wetz JJ, Shipley-Lozano B, Shively JD, Stunz GW (2015) An analysis of artificial reef fish community structure along the northwestern Gulf of Mexico shelf: potential impacts of "Rigs-to-Reefs" programs. PLoS ONE 10(5): e0126354

Akaike H (1974) A new look at the statistical model identification. IEEE Transactions on Automatic Control. 19(6): 716-723

Auster PJ, Malatesta RJ, LaRosa SC (1995) Patterns of microhabitat utilization by mobile megafauna on the southern New England (USA) continental shelf and slope. Marine Ecology Progress Series 127: 77-85

Barry SC, Welsh AH (2002) Generalized additive modelling and zero inflated count data. Ecological Modelling 157(2-3): 179-188

Barton K (2019) Multi-Model Inference. R-CRAN https://cran.r-project.org/web/packages/MuMIn/MuMIn.pdf

Bassett C, De Robertis A, Wilson CD (2018) Broadband echosounder measurements of the frequency response of fishes and euphausiids in the Gulf of Alaska. ICES Journal of Marine Science 75(3):1131-42.

Becker A, Whitfield AK, Cowley PD, Järnegren J, Næsje TF (2011) An assessment of the size structure, distribution and behaviour of fish populations within a temporarily closed estuary using dual frequency identification sonar (DIDSON). Journal of Fish Biology 79(3): 761-775

Benoit-Bird KJ, Waluk CM (2020) Exploring the promise of broadband fisheries echosounders for species discrimination with quantitative assessment of data processing effects. The Journal of the Acoustical Society of America 147(1): 411-427

Boswell KM, Wilson MP, Cowan Jr JH (2008) A semiautomated approach to estimating fish size, abundance, and behavior from dual-frequency identification sonar (DIDSON) data. North American Journal of Fisheries Management 28(3): 799-807

Boswell KM, Wells RJ, Cowan JH, Wilson CA (2010) Biomass, density, and size distributions of fishes associated with a large-scale artificial reef complex in the Gulf of Mexico. Bulletin of Marine Science 86(4): 879-889

Bowler DE, Benton TG (2005) Causes and consequences of animal dispersal strategies: relating individual behaviour to spatial dynamics. Biological Reviews 80(2): 205-225

Buczkowski BJ, Reid JA, Schweitzer PN, Cross VA, Jenkins CJ (2020) usSEABED—Offshore surficial-sediment database for samples collected within the United States Exclusive Economic Zone: U.S. Geological Survey data release, https://doi.org/10.5066/P9H3LGWM

Burnham KP and Anderson DR (2002) Model Selection and Multimodel Inference: A Practical Information-Theoretic Approach. 2nd ed. Springer, Berlin

Chang T, Lin PC, Gao X, Liu F, Duan ZH, Liu HZ (2017) Using adaptive resolution imaging sonar to investigate Chinese sturgeon (*Acipenser sinensis* Gray, 1835) behaviour on its only spawning ground in the Yangtze River. Journal of Applied Ichthyology 33(4): 681-688

Chen X, Lohrenz SE, Wiesenburg DA (2000) Distribution and controlling mechanisms of primary production on the Louisiana–Texas continental shelf. Journal of Marine Systems 25(2): 179-207

Chittenden ME and McEachran JD (1976) Composition, ecology, and dynamics of demersal fish communities on the northwestern Gulf of Mexico continental shelf, with a similar synopsis for the entire Gulf. Texas A&M University Sea Grant. TAMU-SG-76-208: 104

Coetzee J (2000) Use of a shoal analysis and patch estimation system (SHAPES) to characterize sardine schools. Aquatic Living Resources 13(1): 1-10

Craig JK (2012) Aggregation on the edge: effects of hypoxia avoidance on the spatial distribution of brown shrimp and demersal fishes in the Northern Gulf of Mexico. Marine Ecology Progress Series 445: 75-95

Dance MA, Rooker JR (2019) Cross-shelf habitat shifts by red snapper (*Lutjanus campechanus*) in the Gulf of Mexico. PloS ONE 14(3): e0213506

Dennis GD and Bright TJ (1988) Reef fish assemblages on hard banks in the northwestern Gulf of Mexico. Bulletin of Marine Science 43(2): 280-307

De Robertis A, Higginbottom I (2007) A post-processing technique to estimate the signal-to-noise ratio and remove echosounder background noise. ICES Journal of Marine Science 64(6): 1282-1291

Doherty P and Fowler T (1994) An empirical test of recruitment limitation in a coral reef fish. Science 263(5149): 935-939

Dokken QR, Withers K, Childs S, Riggs T (2000) Characterization and comparison of platform reef communities off the Texas coast. Technical report. Center for Coastal Studies, Texas A&M University-Corpus Christi

Ferrari R, Malcolm HA, Byrne M, Friedman A, Williams SB, Schultz A, Jordan AR, Figueira WF (2018) Habitat structural complexity metrics improve predictions of fish abundance and distribution. Ecography 41(7): 1077-1091

Furey NB, Dance MA, Rooker JR (2013) Fine-scale movements and habitat use of juvenile southern flounder *Paralichthys lethostigma* in an estuarine seascape. Journal of Fish Biology 82(5): 1469-1483

Gallaway BJ and Lewbel GS (1982) Ecology of petroleum platforms in the northwestern Gulf of Mexico: a community profile (No. FWS/OBS-82/27). USFWS Office of Biology Services Open File Report 82-03

Gallaway BJ, Szedlmayer ST, Gazey WJ (2009) A life history review for red snapper in the Gulf of Mexico with an evaluation of the importance of offshore petroleum platforms and other artificial reefs. Reviews in Fisheries Science 17(1): 48-67

Gallaway UJ, MF Johnson, LR Martin, FJ Margraf, GS Lewbel, KL Iioward, GS Boland (1981) The artificial reef studies. In Ecological investigations of petroleum production platforms in the central Gulf of Mexico Volume 2. Southwest Research Institute, Houston

Giorli G, Drazen JC, Neuheimer AB, Copeland A, Au WW (2018) Deep sea animal density and size estimated using a dual-frequency identification sonar (DIDSON) offshore the island of Hawaii. Progress in Oceanography 160: 155-166

Gunderson DR, Ellis IE (1986) Development of a plumb staff beam trawl for sampling demersal fauna. Fisheries Research 4(1): 35-41

Hastie T, Tibshirani R (1987) Generalized additive models: some applications. Journal of the American Statistical Association 82(398): 371-386

Hazen EL, Craig JK, Good CP, Crowder LB (2009) Vertical distribution of fish biomass in hypoxic waters on the Gulf of Mexico shelf. Marine Ecology Progress Series 375: 195-207

Herbig JL, Szedlmayer ST (2016) Movement patterns of gray triggerfish, *Balistes capriscus*, around artificial reefs in the northern Gulf of Mexico. Fisheries Management and Ecology 23(5): 418-427

Hewitt JE, Thrush SF, Halliday J, Duffy C (2005) The importance of small-scale habitat structure for maintaining beta diversity. Ecology 86(6): 1619-1626

Holmes JA, Cronkite GM, Enzenhofer HJ, Mulligan TJ (2006) Accuracy and precision of fish-count data from a dual-frequency identification sonar (DIDSON) imaging system. ICES Journal of Marine Science 63(3): 543-555

Horne JK (2000) Acoustic approaches to remote species identification: a review. Fisheries oceanography 9(4): 356-371

Hosmer DW, Lemeshow S (2000) Applied Logistic Regression. John Wiley & Sons, New York

Jing D, Han J, Wang X, Wang G, Tong J, Shen W, Zhang J (2017) A method to estimate the abundance of fish based on dual-frequency identification sonar (DIDSON) imaging. Fisheries science 83(5): 685-697

Kang M, Furusawa M, Miyashita K (2002) Effective and accurate use of difference in mean volume backscattering strength to identify fish and plankton. ICES Journal of Marine Science 59(4): 794-804

Keefer ML, Caudill CC, Johnson EL, Clabough TS, Boggs CT, Johnson PN, Nagy WT (2017) Inter-observer bias in fish classification and enumeration using dual-frequency identification sonar (DIDSON): A pacific lamprey case study. Northwest Science 91(1): 41-53

Kieser R, Mulligan TJ (1984) Analysis of echo counting data: a model. Canadian Journal of Fisheries and Aquatic Sciences 41(3): 451-458

Kotwicki S, Buckley TW, Honkalehto T, Walters G (2005) Variation in the distribution of walleye pollock (*Theragra chalcogramma*) with temperature and implications for seasonal migration. Fishery Bulletin 103(4): 574-587

Langkau MC, Balk H, Schmidt MB, Borcherding J (2012) Can acoustic shadows identify fish species? A novel application of imaging sonar data. Fisheries Management and Ecology 19(4): 313-322

Langton RW, Steneck RS, Gotceitas V, Juanes F, Lawton P (1996) The interface between fisheries research and habitat management. North American Journal of Fisheries Management 16(1): 1-7

Li Y, Nowlin WD, Reid RO (1997) Mean hydrographic fields and their interannual variability over the Texas-Louisiana continental shelf in spring, summer, and fall. Journal of Geophysical Research: Oceans 102(C1): 1027-1049

Lloret J, Gil de Sola L, Souplet A, Galzin R (2002) Effects of large-scale habitat variability on condition of demersal exploited fish in the north-western Mediterranean. ICES Journal of Marine Science 59(6): 1215-1227

Lohrenz SE, Dagg MJ, Whitledge TE (1990) Enhanced primary production at the plume/oceanic interface of the Mississippi River. Continental Shelf Research 10(7): 639-664

Lohrenz SE, Fahnenstiel GL, Redalje DG, Lang GA, Chen X, Dagg MJ (1997) Variations in primary production of northern Gulf of Mexico continental shelf waters linked to nutrient inputs from the Mississippi River. Marine Ecology Progress Series 155: 45-54

Lohrenz SE, Fahnenstiel GL, Redalje DG, Lang GA, Dagg MJ, Whitledge TE, Dortch Q (1999) Nutrients, irradiance, and mixing as factors regulating primary production in coastal waters impacted by the Mississippi River plume. Continental Shelf Research 19(9): 1113-1141

Love RH (1977) Target strength of an individual fish at any aspect. The Journal of the Acoustical Society of America 62(6): 1397-1403

Lugo-Fernández A (1998) Ecological implications of hydrography and circulation to the Flower Garden Banks, northwest Gulf of Mexico. Gulf of Mexico Science 16(2): 4

MacLennan DN, Menz A (1996) Interpretation of in situ target-strength data. ICES Journal of Marine Science 53(2): 233-236

Macpherson E, Duarte CM (1991) Bathymetric trends in demersal fish size: is there a general relationship? Marine Ecology Progress Series 11: 103-112

Martínez-López B, Zavala-Hidalgo J (2009) Seasonal and interannual variability of cross-shelf transports of chlorophyll in the Gulf of Mexico. Journal of Marine Systems 77(1-2): 1-20

McCawley JR, Cowan JH, Shipp RL (2006) Feeding Periodicity and Prey Habitat Preference of Red Snapper, *Lutjanus campechanus* (Poey, 1860) on Alabama Artificial Reefs. Gulf of Mexico Science 24(1): 4

McClatchie S, Thorne RE, Grimes P, Hanchet S (2000) Ground truth and target identification for fisheries acoustics. Fisheries Research 47(2-3): 173-191

Mevik BH, Cederkvist HR (2004) Mean squared error of prediction (MSEP) estimates for principal component regression (PCR) and partial least squares regression (PLSR). Journal of Chemometrics 18(9): 422-429

Molinaro AM, Simon R, Pfeiffer RM (2005) Prediction error estimation: a comparison of resampling methods. Bioinformatics 21(15): 3301-3307

Monk MH, Powers JE, Brooks EN (2015) Spatial patterns in species assemblages associated with the northwestern Gulf of Mexico shrimp trawl fishery. Marine Ecology Progress Series 519: 1-12

Mueller AM, Burwen DL, Boswell KM, Mulligan T (2010) Tail-beat patterns in dual-frequency identification sonar echograms and their potential use for species identification and bioenergetics studies. Transactions of the American Fisheries Society 139(3): 900-910

Ona E, Mitson RB (1996) Acoustic sampling and signal processing near the seabed: the deadzone revisited. ICES Journal of Marine Science53(4): 677-690

Parker RO, Colby DR, Willis TD (1983) Estimated amount of reef habitat on a portion of the US South Atlantic and Gulf of Mexico continental shelf. Bulletin of Marine Science 33(4): 935-940

Parker-Stetter SL, Rudstam LG, Sullivan PJ, Warner DM (2009) Standard operating procedures for fisheries acoustics in the Great Lakes, version 1.0. Great Lakes Fisheries Commission Special Publication.

Patterson WF, Wilson CA, Bentley SJ, Cowan JH Jr, Henwood T, Allen YC, Dufrene TA (2005) Delineating juvenile red snapper habitat on the northern Gulf of Mexico continental shelf. In: Barnes PW, Thomas JP (eds) Benthic habitats and the effects of fishing. American Fisheries Society Symposium 41: 277–288

Peabody MB and Wilson CA (2006) Fidelity of Red Snapper (*Lutjanus campechanus*) to petroleum platforms and artificial reefs in the northern Gulf of Mexico. U.S. Department of the Interior, Minerals Management Service, Gulf of Mexico Outer Continental Shelf Region, OCS Study MMS-2006-005

Plumlee JD, Dance KM, Dance MA, Rooker JR, TinHan TC, Shipley JB, Wells RJD (2020) Fish assemblages associated with artificial reefs assessed using multiple gear types in the northwest Gulf of Mexico. Bulletin of Marine Science 96 (preprint)

R Core Team (2020) R: A language and environment for statistical computing. R Foundation for Statistical Computing, Vienna, Austria. URL https://www.R-project.org/

Rabalais NN, Turner RE, Wiseman Jr WJ (2002) Gulf of Mexico hypoxia, aka "The dead zone". Annual Review of Ecology and Systematics 33(1): 235-263

Rezak R, Gittings SR, Bright TJ (1990) Biotic assemblages and ecological controls on reefs and banks of the northwest Gulf of Mexico. American Zoologist 30(1): 23-35

Rooker JR, Landry AM, Geary BW, Harper JA (2004) Assessment of a shell bank and associated substrates as nursery habitat of postsettlement red snapper. Estuarine Coastal and Shelf Science 59: 653-661

Rooker JR, Dance MA, Wells RD, Quigg A, Hill RL, Appeldoorn RS, Padovani Ferreira B, Boswell KM, Sanchez PJ, Moulton DL, Kitchens LL (2018) Seascape connectivity and the influence of predation risk on the movement of fishes inhabiting a back-reef ecosystem. Ecosphere 9(4): 2200

Rudstam LG, Jech JM, Parker-Stetter SL, Horne JK, Sullivan PJ, Mason DM (2012) Fisheries acoustics. In Fisheries Techniques, third edition. pp 597-636. American Fisheries Society, Bethesda

Ryer CH, Laurel BJ, Stoner AW (2010) Testing the shallow water refuge hypothesis in flatfish nurseries. Marine Ecology Progress Series 415: 275-282

Sala E, Ballesteros E, Starr RM (2001) Rapid decline of Nassau grouper spawning aggregations in Belize: fishery management and conservation needs. Fisheries 26(10): 23-30

Salmerón-García O, Zavala-Hidalgo J, Mateos-Jasso A, Romero-Centeno R (2011) Regionalization of the Gulf of Mexico from space-time chlorophyll-a concentration variability. Ocean Dynamics 61(4): 439-48

Sawada K, Furusawa M, Williamson NJ (1993) Conditions for the precise measurement of fish target strength in situ. Journal of the Marine Acoustical Society of Japan 20: 73-79

Schmahl GP, Hickerson EL, Precht WF (2008) Biology and ecology of coral reefs and coral communities in the Flower Garden Banks region, northwestern Gulf of Mexico. In Coral Reefs of the USA 2008 pp. 221-261. Springer, Dordrecht.

Schultz AL, Malcolm HA, Bucher DJ, Smith SD (2012) Effects of reef proximity on the structure of fish assemblages of unconsolidated substrata. PloS ONE 7(11)

Schultz AL, Malcolm HA, Bucher DJ, Linklater M, Smith SD (2014) Depth and medium-scale spatial processes influence fish assemblage structure of unconsolidated habitats in a subtropical marine park. PloS ONE 9(5)

Simmonds J and MacLennan D (2005) Fisheries Acoustics: Theory and Practice. 2nd Ed. John Wiley and Sons.

Sing T, Sander O, Beerenwinkel N, Lengauer T (2005) ROCR: visualizing classifier performance in R. Bioinformatics 21(20): 7881. http://rocr.bioinf.mpi-sb.mpg.de

Soule M, Barange M, Solli H, Hampton I (1997) Performance of a new phase algorithm for discriminating between single and overlapping echoes in a split-beam echosounder. ICES Journal of Marine Science 54(5): 934-938

Stanley DR and Wilson CA (1997) Seasonal and spatial variation in the abundance and size distribution of fishes associated with a petroleum platform in the northern Gulf of Mexico. Canadian Journal of Fisheries and Aquatic Sciences 54(5): 1166-1176

Streich MK, Ajemian MJ, Wetz JJ, Stunz GW (2017) A comparison of fish community structure at mesophotic artificial reefs and natural banks in the western Gulf of Mexico. Marine and Coastal Fisheries 9(1): 170-189

Thrush SF, Hewitt JE, Funnell GA, Cummings VJ, Ellis J, Schultz D, Talley D, Norkko A (2001) Fishing disturbance and marine biodiversity: role of habitat structure in simple soft-sediment systems. Marine Ecology Progress Series 221: 255-264

Thrush SF, Schultz D, Hewitt JE, Talley D (2002) Habitat structure in soft-sediment environments and abundance of juvenile snapper *Pagrus auratus*. Marine Ecology Progress Series 245: 273-280

Vickery K (1998) Acoustic positioning systems. A practical overview of current systems. Proceedings of the 1998 Workshop on Autonomous Underwater Vehicles (Cat. No. 98CH36290)

Walker ND, Wiseman Jr WJ, Rouse Jr LJ, Babin A (2005) Effects of river discharge, wind stress, and slope eddies on circulation and the satellite-observed structure of the Mississippi River plume. Journal of Coastal Research 21(6): 1228-1244

Wells RD, Cowan Jr JH, Fry B (2008a) Feeding ecology of red snapper Lutjanus campechanus in the northern Gulf of Mexico. Marine Ecology Progress Series 361: 213-225

Wells RD, Cowan JH, Patterson WF, Walters CJ (2008b) Effect of trawling on juvenile red snapper (*Lutjanus campechanus*) habitat selection and life history parameters. Canadian Journal of Fisheries and Aquatic Sciences. Marine Ecology Progress Series 361: 213-225

Wells RD, Harper JO, Rooker JR, Landry AM, Dellapenna TM (2009) Fish assemblage structure on a drowned barrier island in the northwestern Gulf of Mexico. Hydrobiologia 625: 207-221

Williams-Grove LJ, Szedlmayer ST (2016) Acoustic positioning and movement patterns of red snapper *Lutjanus campechanus* around artificial reefs in the northern Gulf of Mexico. Marine Ecology Progress Series 553: 233-251

Williams-Grove LJ, Szedlmayer ST (2017) Depth preferences and three-dimensional movements of red snapper, Lutjanus campechanus, on an artificial reef in the northern Gulf of Mexico. Fisheries Research 190: 61-70

Wilson CA, Pierce A, Miller MW (2003) Rigs and reefs: a comparison of the fish communities at two artificial reefs, a production platform, and a natural reef in the northern Gulf of Mexico. Prepared by the Coastal Fisheries Institute, School of the Coast and Environment. Louisiana State University. US Dept. of the Interior, Minerals Mgmt. Service.

Wood S (2019) Mixed GAM Computation Vehicle. R-CRAN https://cran.r-project.org/web/packages/mgcv/mgcv.pdf

Wood SN, Goude Y, Shaw S (2015) Generalized additive models for large data sets. Journal of the Royal Statistical Society: Series C (Applied Statistics) 64(1): 139-155

Zimmermann M (2003) Calculation of untrawlable areas within the boundaries of a bottom trawl survey. Canadian Journal of Fisheries and Aquatic Sciences 60(6): 657-669

Zuur A, Ieno EN, Walker N, Saveliev AA, Smith GM (2009) Mixed effects models and

extensions in ecology with R. Springer Science & Business Media, New York

APPENDIX A

TABLES

Table 1. Explanatory variables considered for inclusion in the binomial and Gaussian GAM selection process, including any transformations applied to the data and their sources. Binomial GAM Selection and Gaussian GAM Selection columns indicate whether variables were eliminated from selection for explaining less than one percent of the deviance (<1% DE), eliminated due to correlation with a more highly explanatory variable (* followed by the correlated variable), or whether they were included in the final model (**Included**).

	Units	Transformation	Source	Binomial GAM Selection	Gaussian GAM Selection
Temporal					
Day of year	Days	None	-	*SST	*SST
Environmental					
Distance to shore	m	Log(x)		*Depth	*Depth
Depth	m	None	GEODAS US Coastal Relief Model	**Included**	**Included**
Chlorophyll-a concentration	mg/m^3	Log(x)	VIIRS Multi-Sensor Gap-Filled Chlorophyll	*Depth	*Depth
Chlorophyll-a monthly average	mg/m^3	Log(x)	VIIRS Multi-Sensor Gap-Filled Chlorophyll	*Depth	*Depth
Chlorophyll-a 3-month average	mg/m^3	Log(x)	VIIRS Multi-Sensor Gap-Filled Chlorophyll	*Depth	*Depth
Bottom Rock Composition	% Rock	Log(x+1)	USSeaBed	<1% DE	**Included**
Sea Surface Temperature (SST)	°C	None	NOAA Coastwatch	**Included**	**Included**
Sea Surface Salinity	PSU	None	HYCOM	**Included**	**Included**
Relief Anomaly Variables					
Relief Anomaly Linear Proportion (RALP)	None	Log(x+0.0001)	Echograms	**Included**	*µRA Len.
Mean Relief Anomaly Length (µRA Len.)	m	Log(x+1)	Echograms	*RALP	**Included**
Max Relief Anomaly Length	m	Log(x+1)	Echograms	*RALP	*µRA Len.
Mean Relief Anomaly Height	m	Log(x+1)	Echograms	*RALP	<1% DE
Max Relief Anomaly Height	m	Log(x+1)	Echograms	*RALP	<1% DE

Feature Proximity

Distance to pipeline	m	Log(x+1)	BOEM	<1% DE	**Included**
Distance to active petroleum platforms	m	Log(x+1)	BOEM	**Included**	**Included**
Distance to artificial structure	m	Log(x+1)	NOAA Office of Coastal Survey, TPWD	**Included**	**Included**
Distance to hardbottom habitat	m	Log(x+1)	M. Streich (pers. comm)	**Included**	**Included**

Table 2. Summary of fishes identified from camera transects, including their counts, the number of transects in which they were detected and the frequency of occurrence in transects.

Family	Species	Count	n Transects	Freq. of. Occ.
Balistidae (Triggerfishes)	*Balistes capriscus* (Grey triggerfish)	1	1	1.6%
Carangidae (Jacks)	Unknown	12	5	8.2%
-	*Decapterus sp.* (Round scads)	40	1	1.6%
-	*Caranx crysos* (Blue runner)	6	1	1.6%
Carcharhinidae (Requiem sharks)	Unknown	29	6	9.8%
Echeneidae (Remoras)	Unknown	9	5	8.2%
Lutjanidae (Snappers)	Unknown	3	1	1.6%
-	*Lutjanus campechanus* (Red snapper)	241	11	18.0%
Rachycentridae (Cobia)	Unknown	5	1	1.6%
Scombridae (Tunas/Mackerals)	Unknown	87	7	11.5%
Unknown	Unknown	91	14	23.0%

Table 3. Contingency table showing the agreement of the echo sounder (ES) and imaging sonar at detecting fish in transects. Bold numbers on the diagonal show the number of transects where the gears agreed on fish detection, italic numbers show the number of transects in which one gear detected fish and the other did not. Marginal row/column percentages show the probability of gear agreement in that row/column; The percentage in the bottom right hand corner is the overall percentage of agreement.

		Imaging Sonar		
		Present	Absent	
ES	Present	**40**	*1*	98%
	Absent	*1*	**2**	66%
		98%	66%	95%

Table 4. Contingency table showing the agreement of the echo sounder (ES) and imaging sonar at detecting relief anomalies in transects. Bold numbers on the diagonal show the number of transects where the gears agreed on relief anomaly detection, italic numbers show the number of transects in which one gear detected relief anomaly and the other did not. Marginal row/column percentages show the probability of gear agreement in that row/column; The percentage in the bottom right hand corner is the overall percentage of agreement.

		Imaging Sonar		
		Present	Absent	
ES	Present	**27**	*10*	73%
	Absent	*5*	**2**	29%
		84%	17%	66%

Table 5. Summary of the terms included in the final binomial model of fish presence/absence. EDF = effective degrees of freedom of the smooth term; X^2 = Chi-square test statistic of the smooth term; p-value = probability of the calculated test statistic, under a null hypothesis of no term effect; ΔDE = loss of deviance explained from removing the variable from the model; ΔAIC = increase in AIC from removing the variable from the model

Smooth Term	EDF	X^2	p-value	ΔDE	ΔAIC
s(Depth)	2.882	289.29	< 0.001	5.7%	247.1
s(RALP)	2.548	197.4	< 0.001	5.0%	218.5
s(SST)	2.916	66.68	< 0.001	1.7%	72.8
s(Dist. Art. Structure)	1	48.23	< 0.001	1.1%	47.2
s(SSS)	2.549	37.26	< 0.001	1.0%	39.7
s(Dist. Platform)	2.111	12.37	< 0.01	0.4%	13.1

Table 6. Summary of the terms included in the final Gaussian model of logged fish density. EDF = effective degrees of freedom of the smooth term; F = test statistic of the smooth term; p-value = probability of the calculated test statistic, under a null hypothesis of no term effect; ΔDE = Loss of deviance explained from removing the variable from the model; ΔAIC = Increase in AIC from removing the variable from the model

Smooth Term	EDF	F	p-value	ΔDE	ΔAIC
s(Depth)	2.982	251.411	< 0.001	27.8%	538.9
s(Mean Relief Anomaly Length)	2.845	8.321	< 0.001	1.3%	24.0
s(SSS)	2.741	6.477	< 0.001	0.8%	16.2

Table 7. Coverage by area and percentage of each level of predicted UBH quality by depth zone. Note that the first depth zone does not span 20m.

	Areal Coverage (km2) by Category				Percentage by Category			
Depth Zone	**Poor**	**Fair**	**Good**	**Excellent**	**Poor**	**Fair**	**Good**	**Excellent**
10-20	0	0	10	11588	0.0%	0.0%	0.1%	99.9%
20-40	0	5089	13074	1498	0.0%	25.9%	66.5%	7.6%
40-60	5045	6977	0	0	42.0%	58.0%	0.0%	0.0%
60-80	5481	1018	0	0	84.3%	15.7%	0.0%	0.0%
80-100	2560	2	0	0	99.9%	0.1%	0.0%	0.0%

APPENDIX B

FIGURES

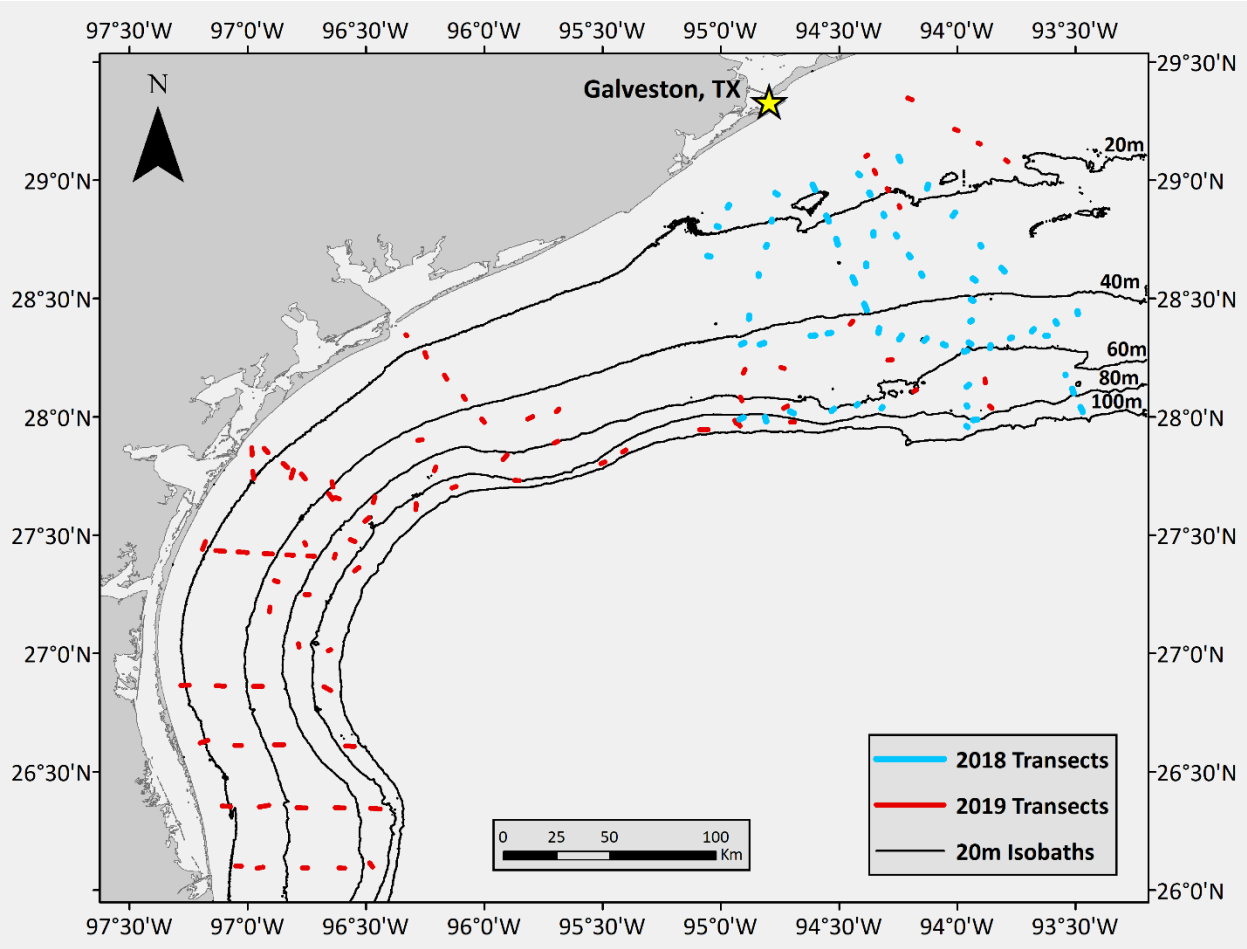

Fig. 1: Location, year and survey extent of the 147 echo sounder transects conducted in this study.

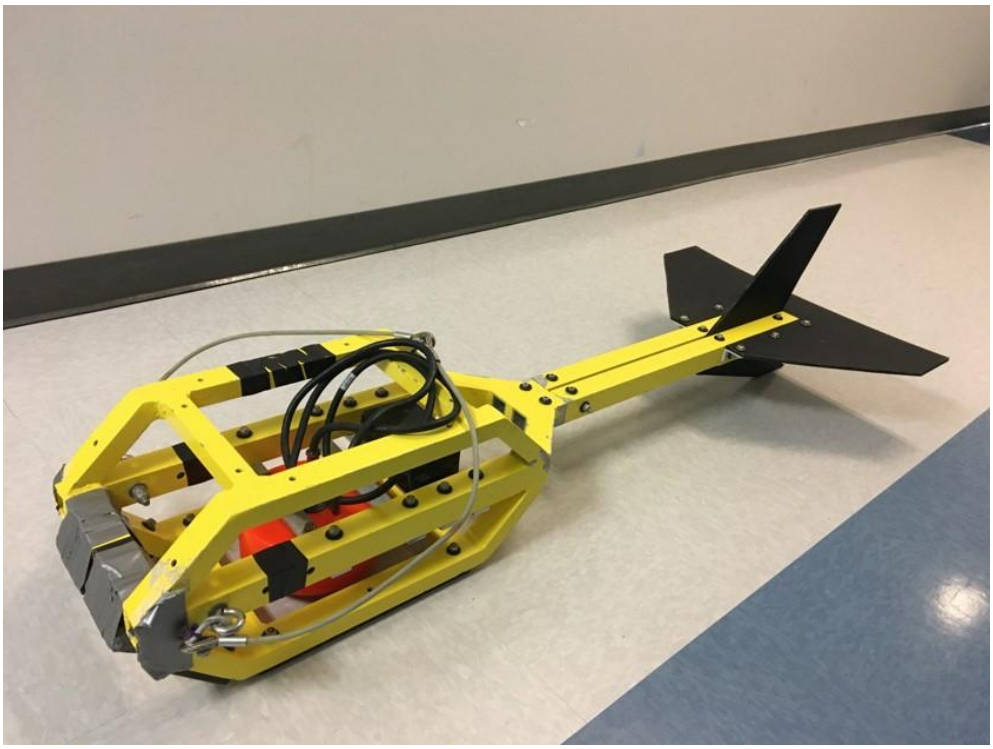

Fig. 2: Tow body for the echo sounder transducer (orange cylinder at frame center).

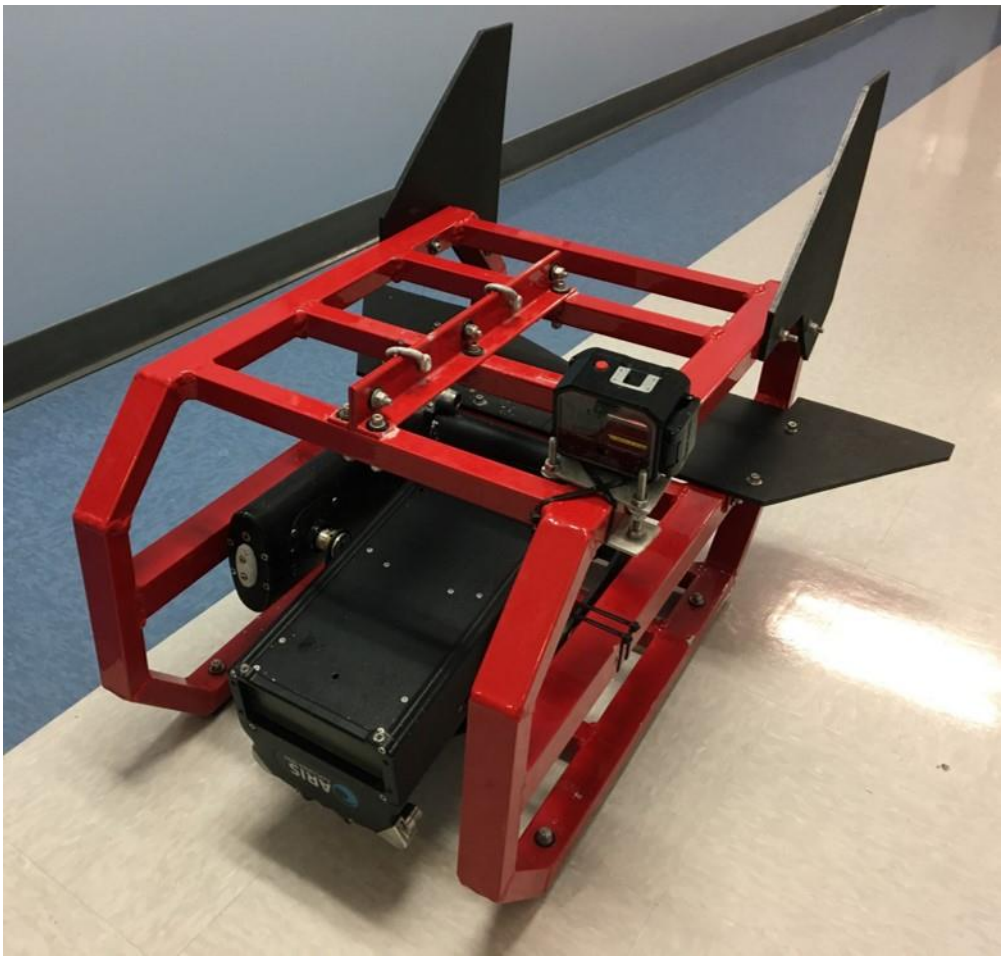

Fig. 3: Video collection tow body for the imaging sonar unit and the standard cameras.

Fig. 4: Standard camera video collection tow body deployed during 2018.

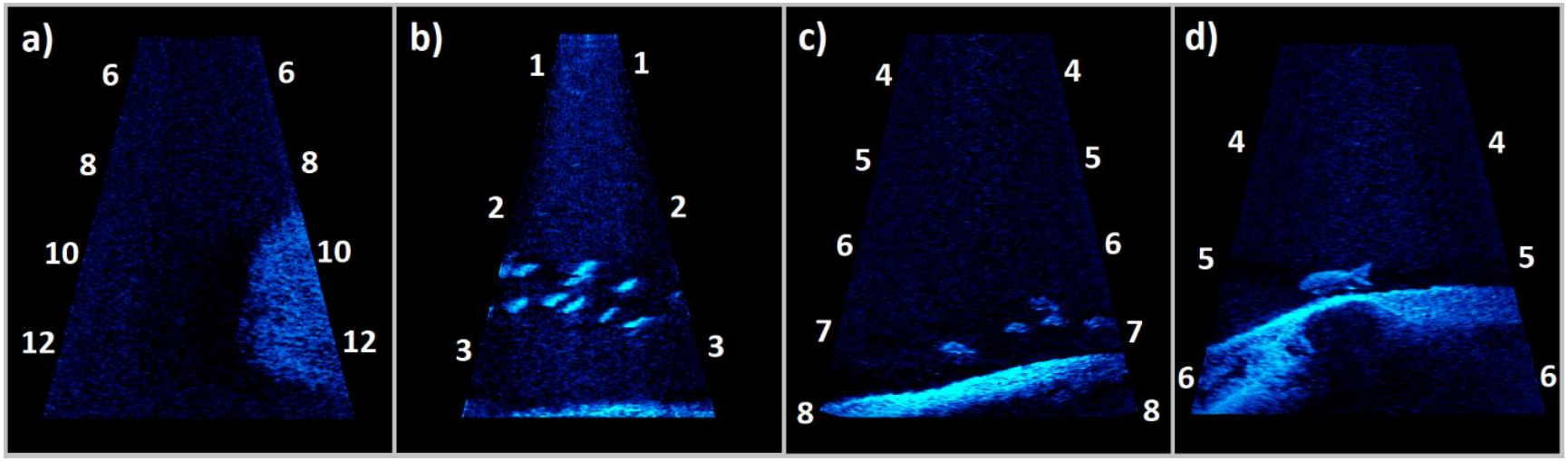

Fig. 5: Examples of fish size categories as determined from the imaging sonar video: **a)** a school of micro fish; **b)** small fish; **c)** medium fish; **d)** a large fish. Numbering shows range from the sonar unit in m.

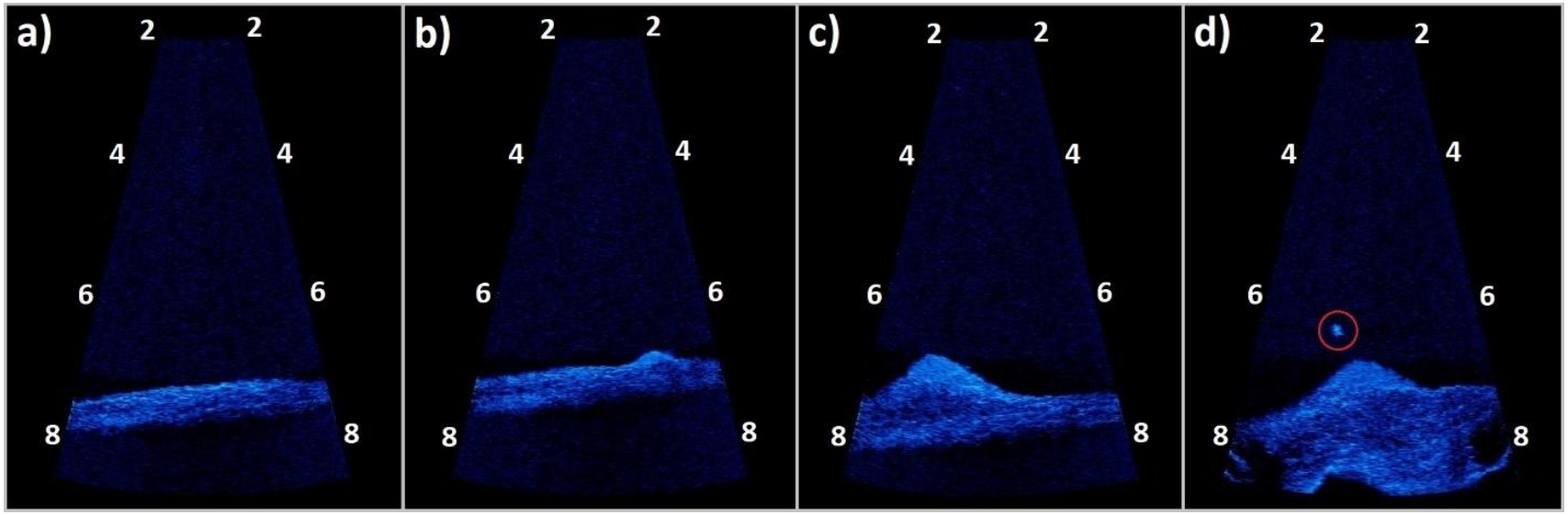

Fig. 6: Examples of semi-quantitative relief anomaly categories as determined from the imaging sonar video: **a)** open bottom, no relief anomalies; **b)** small relief anomaly; **c)** medium relief anomaly; and **d)** large relief anomaly, with a demersal fish in frame (red circle). Numbering shows range from the sonar unit in m.

Fig. 7: Examples of identifiability of fish detected in the standard camera video. **a)** Shows an example of two fish identifiable to species (*Lutjanus campechanus*); **b)** shows a fish identifiable to family (Carcharhinidae); **c)** shows an unidentifiable fish target.

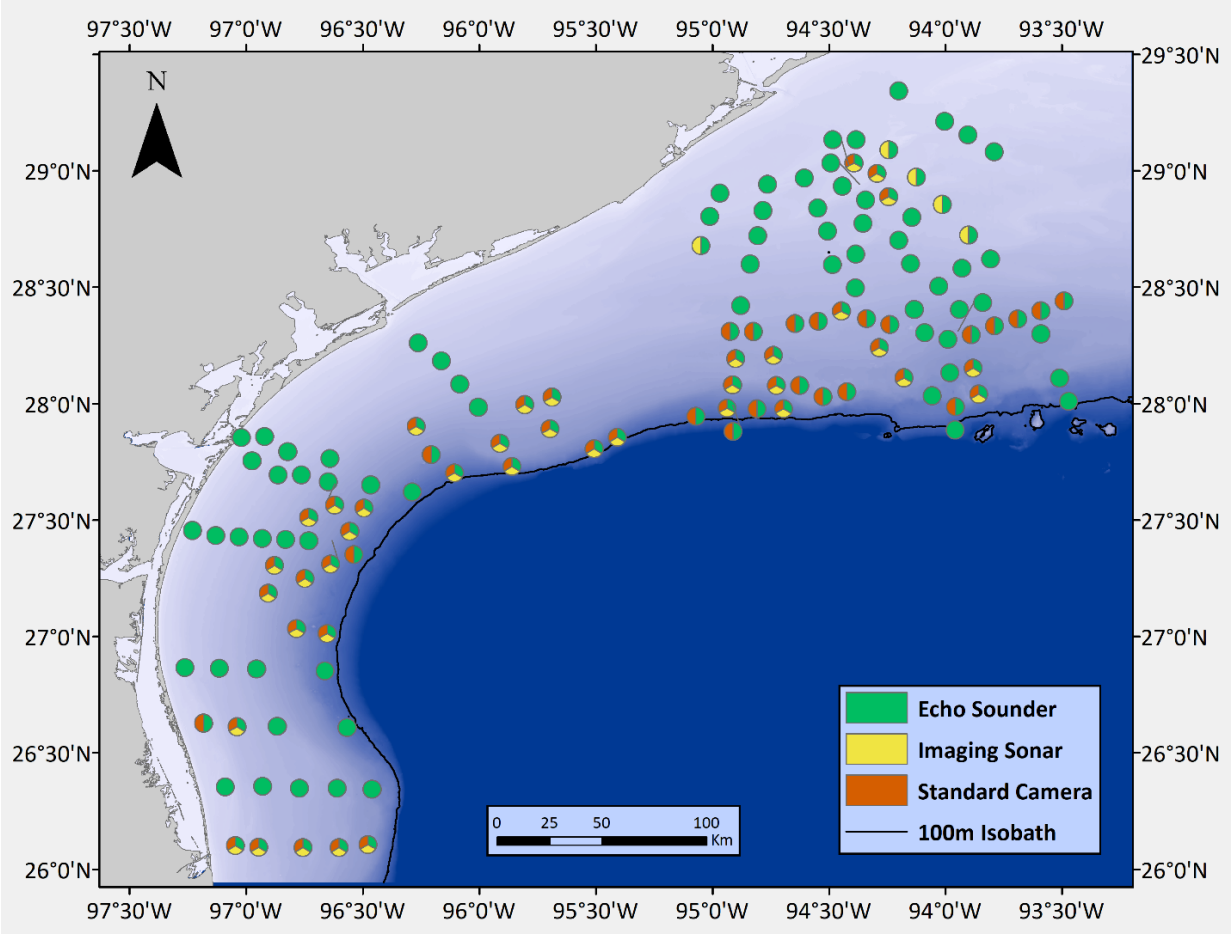

Fig. 8: Locations of the 140 transects on UBH on the continental shelf off Texas in the NGoM used for data analysis. Symbol colors denote which gear types were deployed at each station. The solid black line marks the 100m isobath.

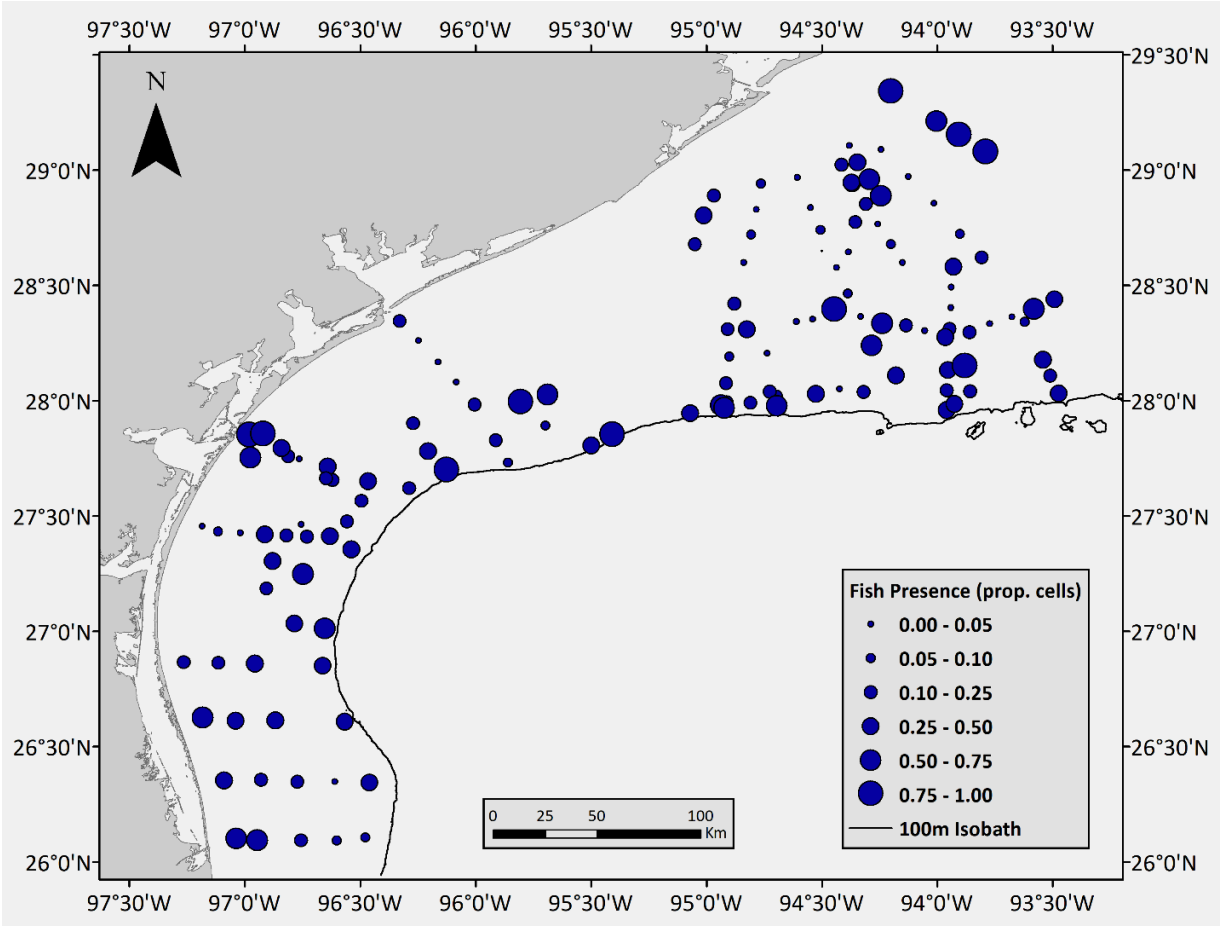

Fig. 9: Proportion of 90m x 20m grid cells where demersal fishes were detected for each transect on UBH on the continental shelf off Texas in the NGoM

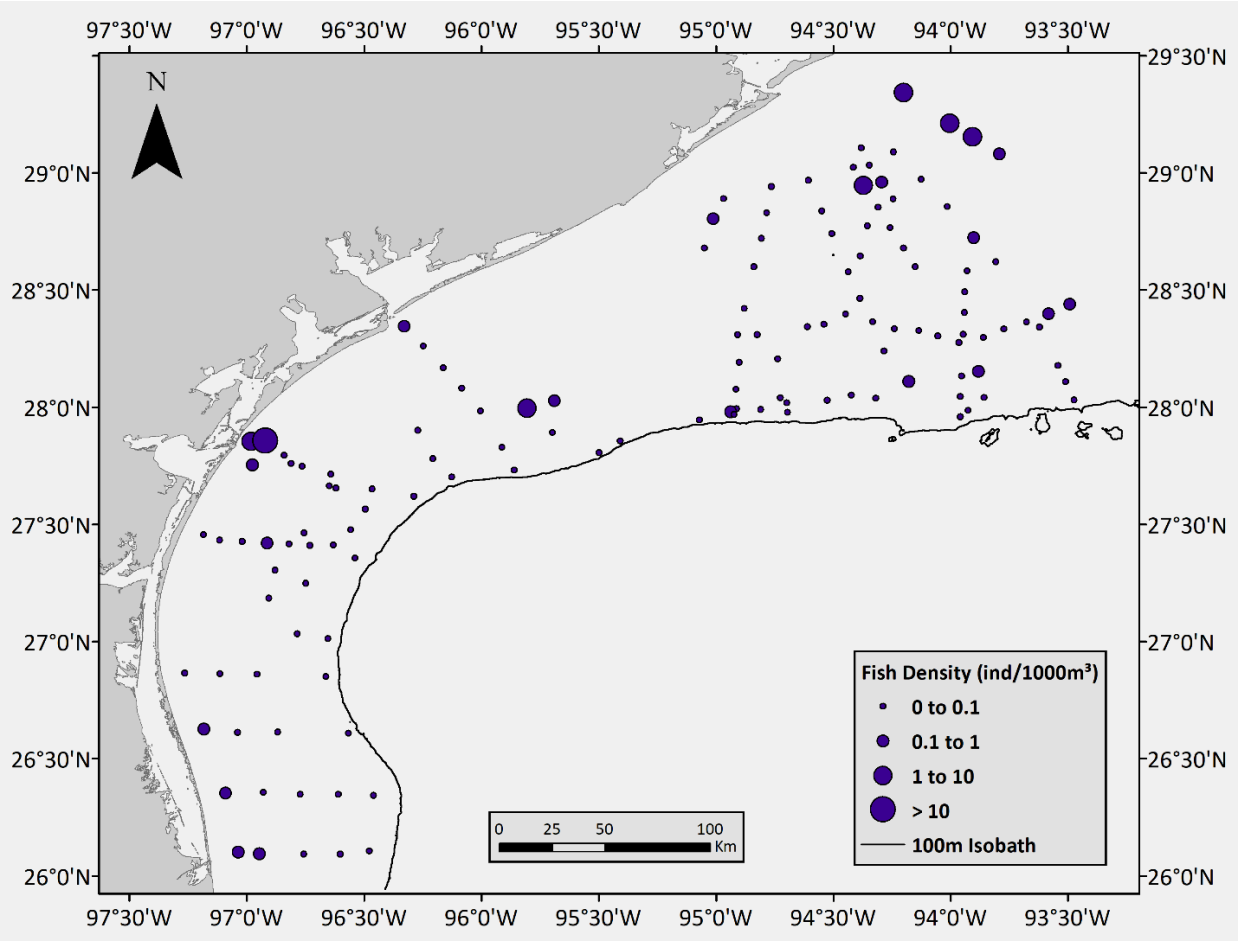

Fig. 10: Density of demersal fishes (ind./1000m^3) from echo sounder transects of UBH on the continental shelf off Texas in the NGoM.

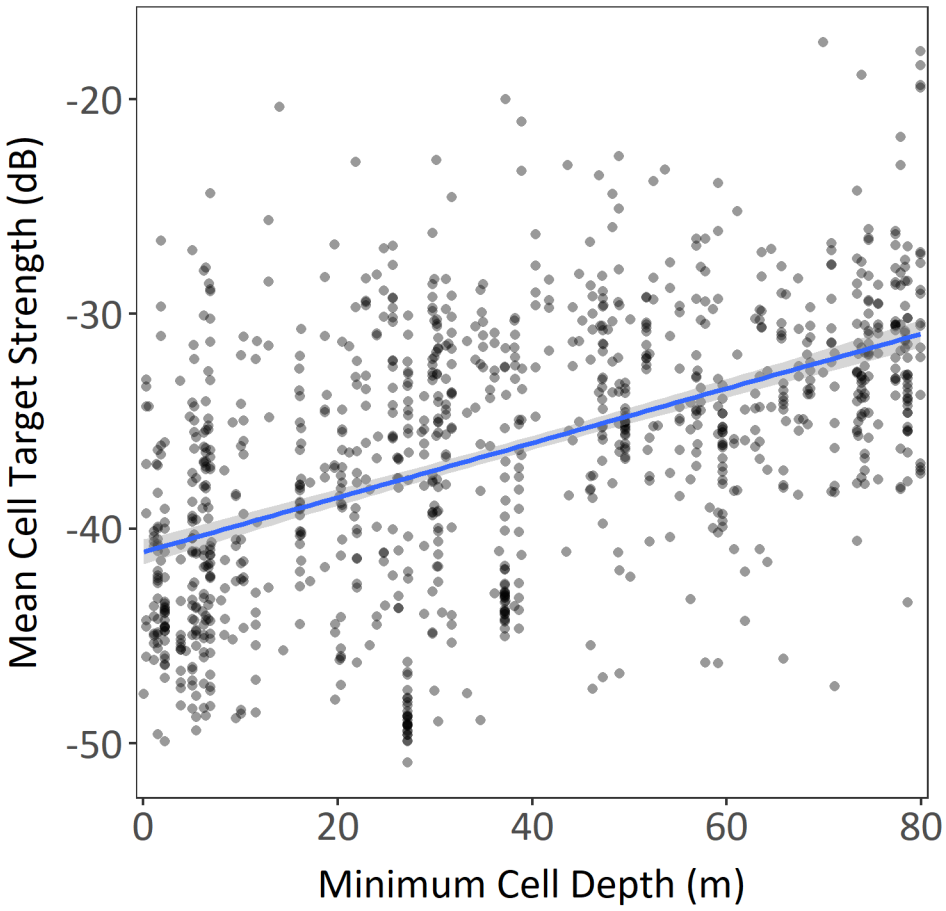

Fig. 11. Mean target strength (TS, in dB) in grid cell versus the minimum cell depth (m) for all cells which had any TS measurement (n = 1022). The fitted linear model has the equation TS_{μ} = -41 + 0.12 x Depth (R^2 = 0.26, F-test p-value < 0.0001).

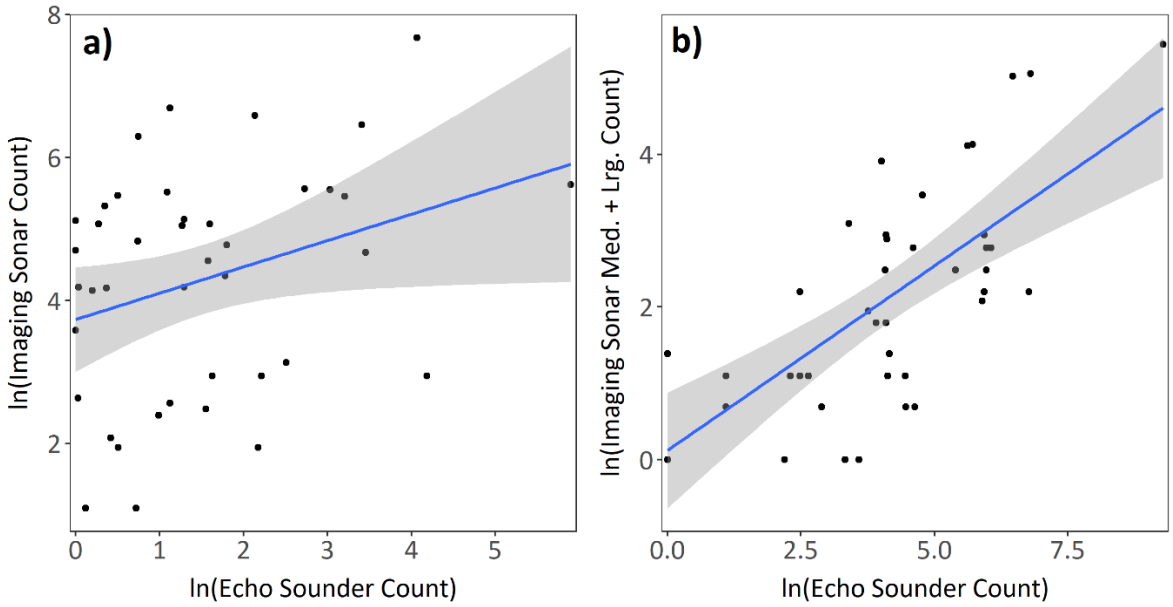

Fig. 12: Fish enumeration comparison between the echo sounder and imaging sonar **a)** Log-transformed total echo sounder target abundance vs. imaging sonar target count; **b)** Log-transformed total echo sounder target abundance vs. summed imaging sonar medium and large target counts. Blue line shows a linear regression; Grey shading denotes a 95% CI.

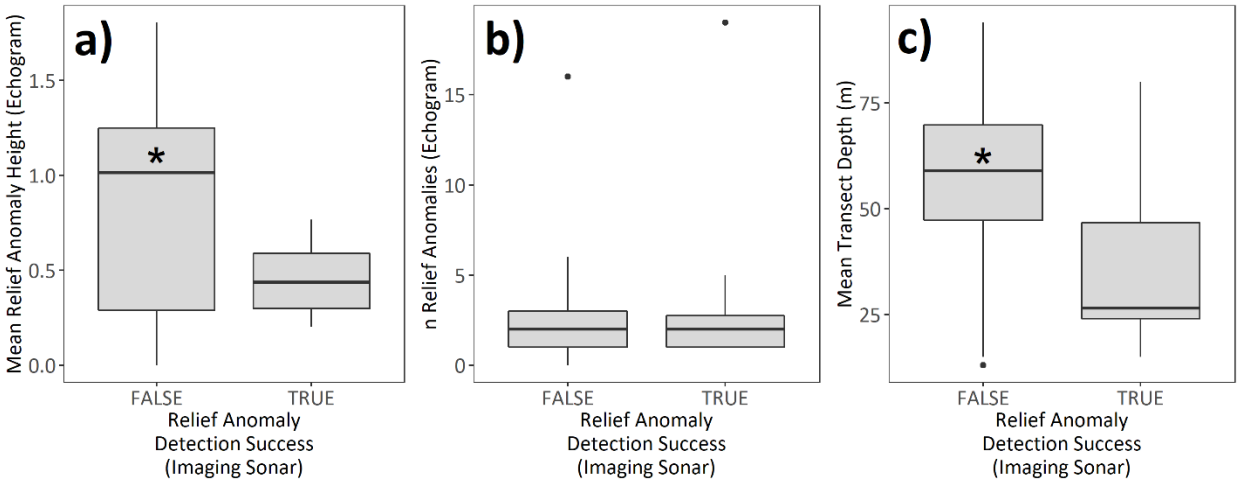

Fig. 13: Boxplots comparing **a)** Mean ES relief anomaly height; **b)** Number of relief anomalies and **c)** Depth, stratified by the success (TRUE) or failure (FALSE) of the imaging sonar to detect relief anomalies. ***** denote means which are significantly different at $\alpha = 0.05$ (Welch's 2-sample t-test).

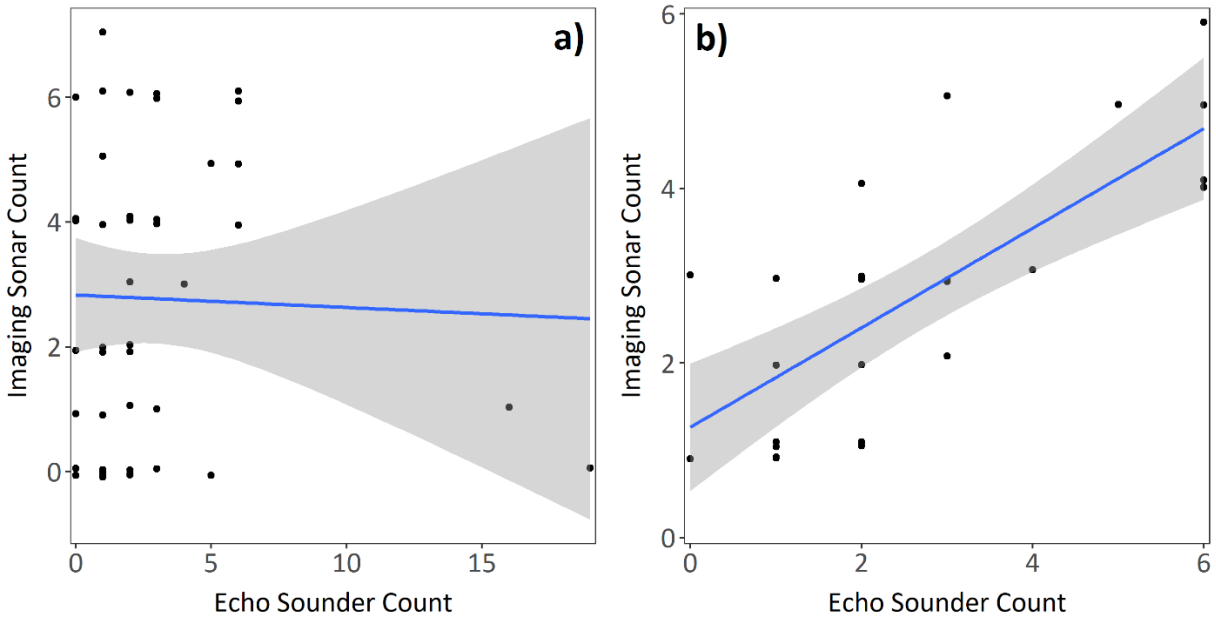

Fig. 14: Relief anomaly enumeration comparison between the echo sounder and imaging sonar; **a)** Echo sounder total relief anomaly count vs. imaging sonar total relief anomaly count; **b)** echo sounder total relief anomaly count vs. imaging sonar relief anomaly count, with the smallest imaging sonar relief anomaly class omitted. Points falling on the same coordinates have a slight vertical jitter. Blue line shows a linear regression; Grey shading denotes a 95% CI.

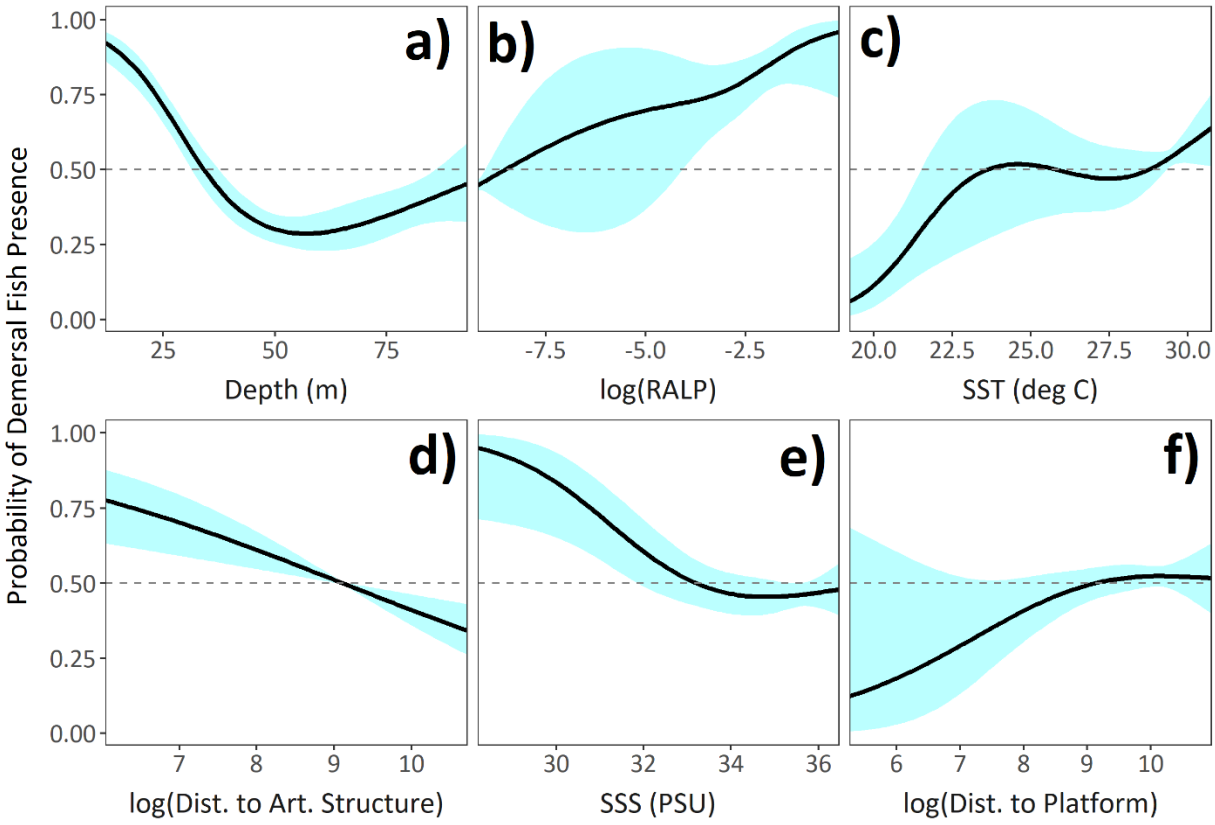

Fig. 15: Response plots for the binomial GAM of demersal fish presence/absence for a) depth; b) logged relief anomaly linear proportion (RALP); c) sea surface temperature (SST); d) logged distance to artificial structure; e) sea surface salinity (SSS); f) logged distance to petroleum platforms. Blue shading shows a 95% CI.

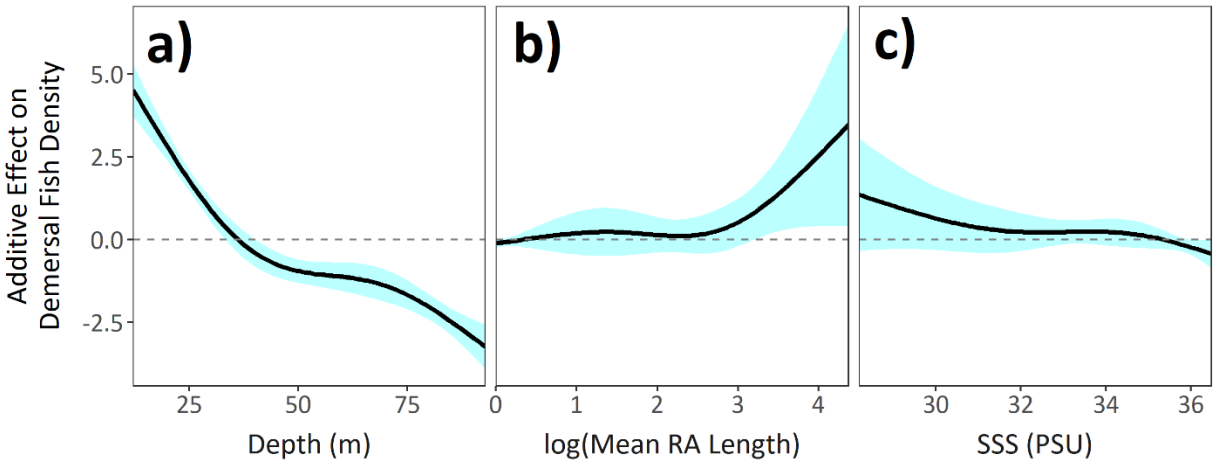

Fig. 16: Response plots for the Gaussian GAM for the effect on transect logged fish density of **a)** depth; **b)** logged mean relief anomaly (RA) feature length; **c)** sea surface salinity (SSS). Blue shading shows a 95% CI.

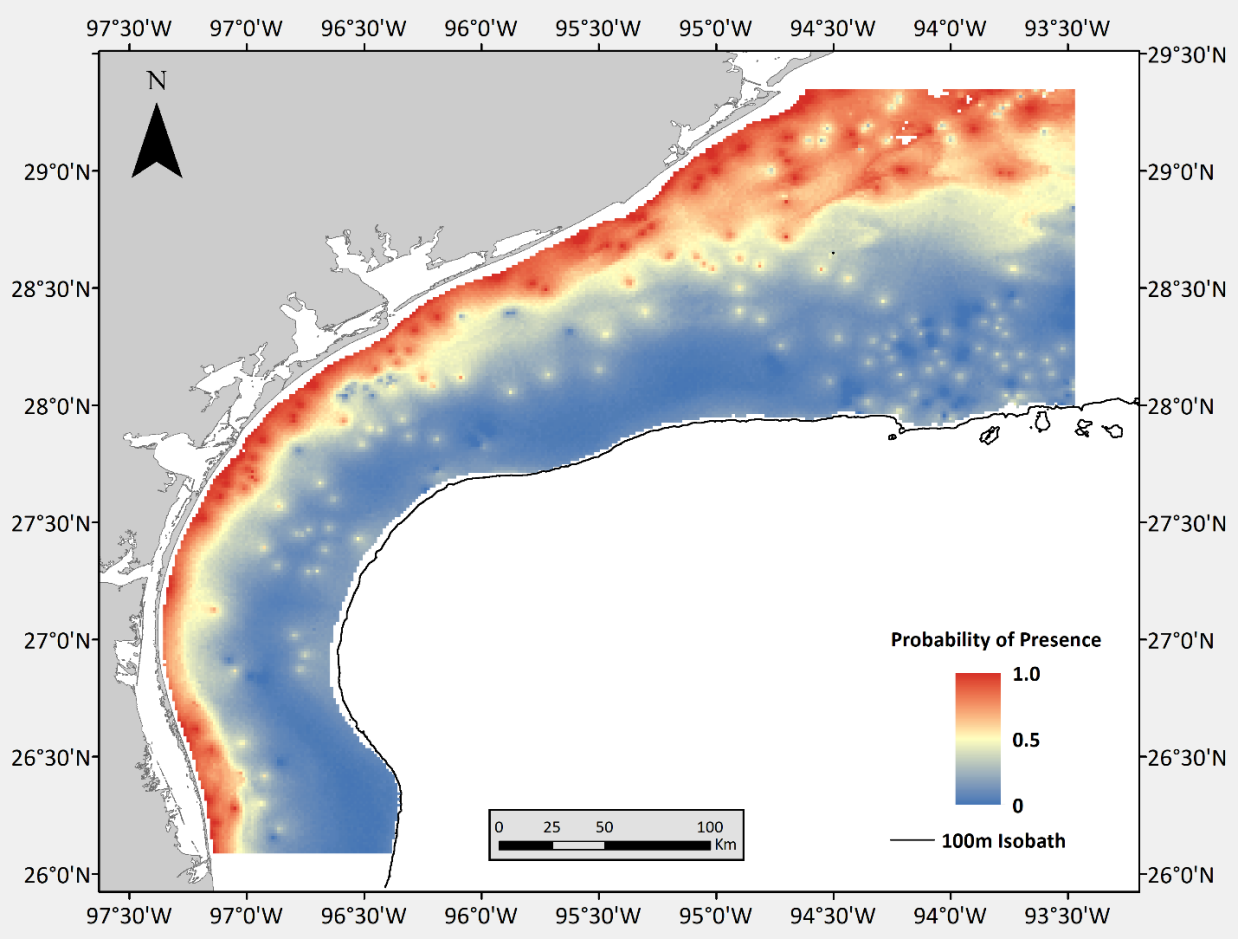

Fig. 17: Visualization of the binomial GAM of demersal fish presence/absence on UBH on the continental shelf off Texas in the NGoM. Predictions were generated over a 0.0125° x 0.0125° grid. Blues indicate a predicted probability of presence <0.5, reds indicated a predicted probability of presence >0.5.

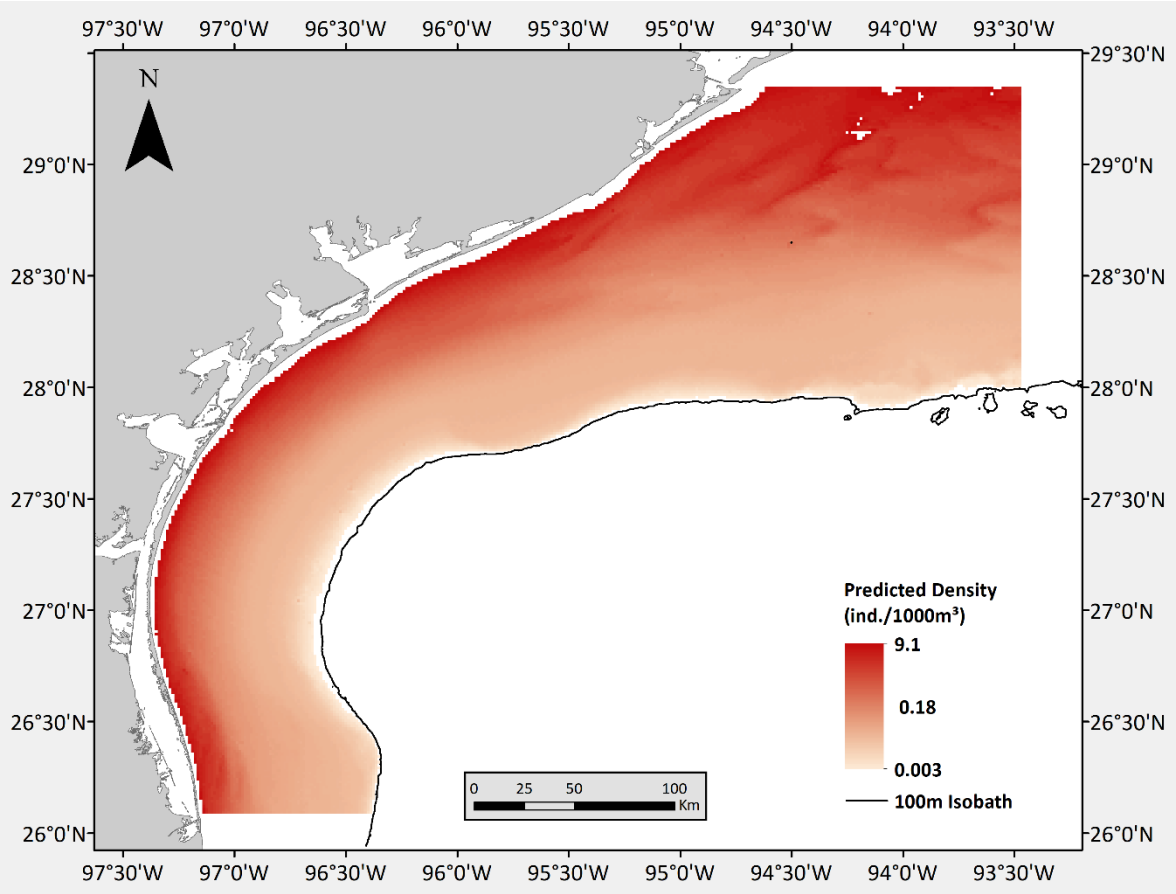

Fig. 18: Visualization of the Gaussian GAM of demersal fish density on UBH on the continental shelf off Texas in the NGoM. Predictions were generated for a 0.0125° x 0.0125° grid. Darker reds indicate higher predicted demersal fish density. Logged density predictions were back-transformed to linear values for visualization.

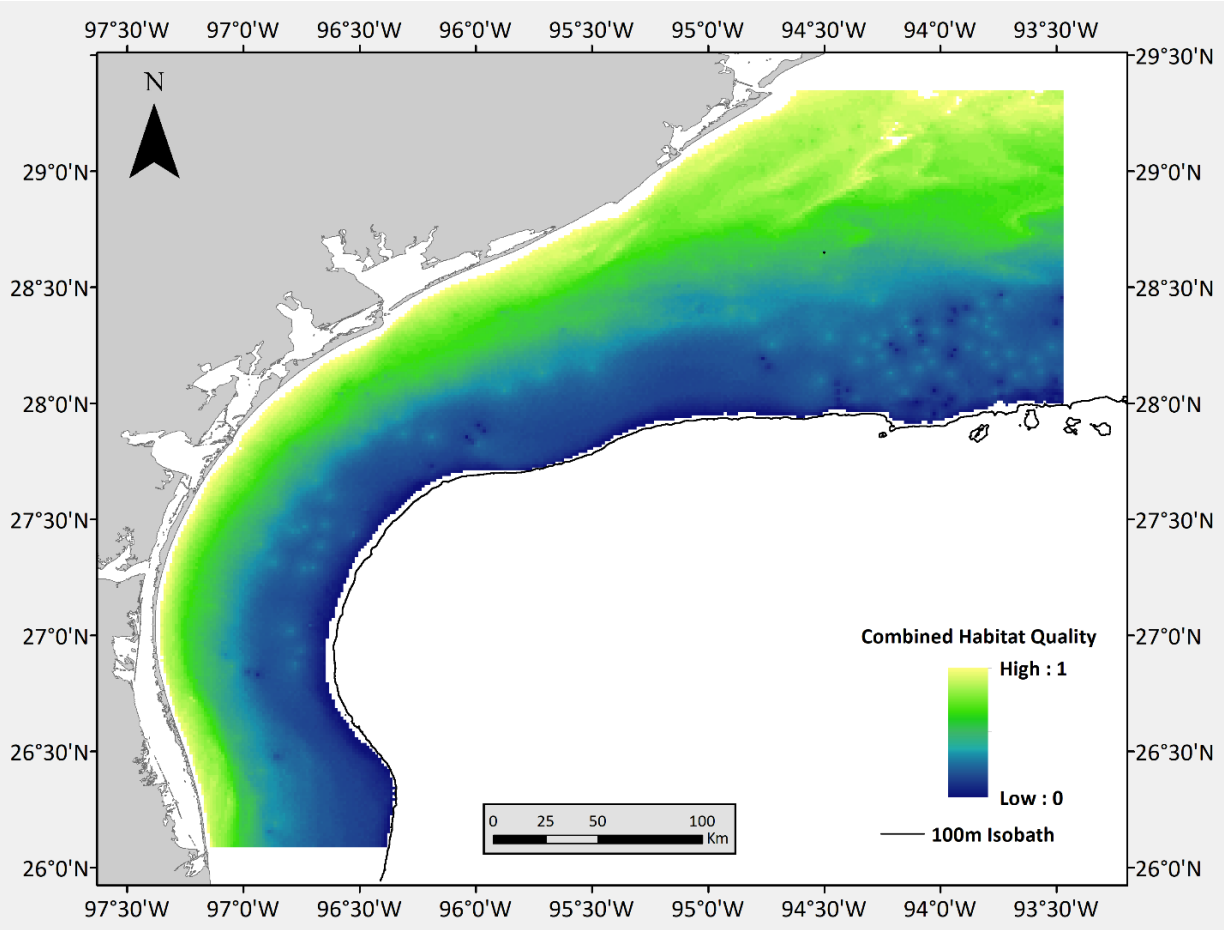

Fig. 19: Combined binomial GAM and Gaussian GAM predictions of UBH demersal fish habitat quality on the continental shelf off Texas in the NGoM. Values were standardized to a 0-1 range between the minimum and maximum prediction values. Yellow indicates areas where high-quality UBH is predicted; Blue indicates areas where UBH quality is predicted to be lower.

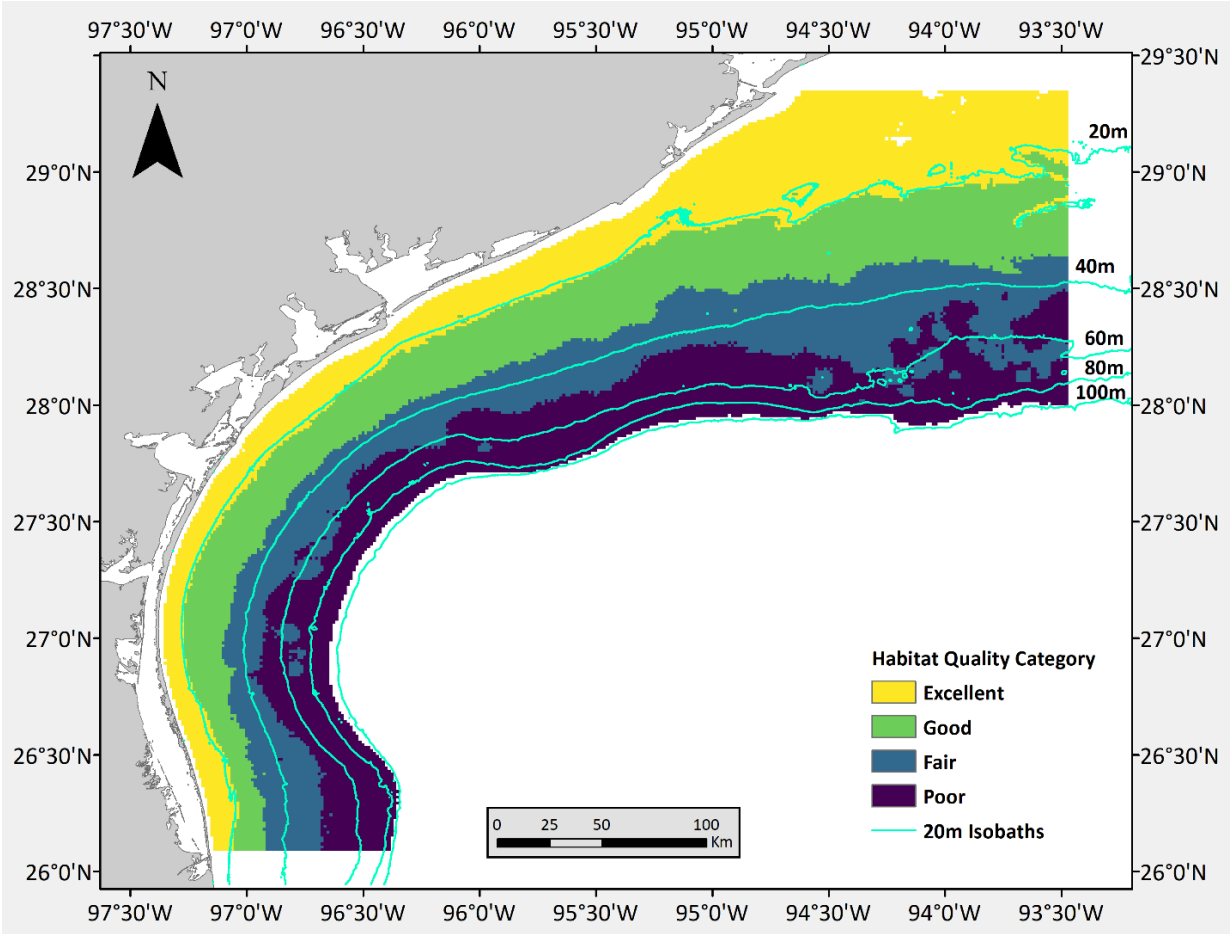

Fig. 20: UBH quality visualized by category, with each category containing a quarter of the data. Cyan lines show 20m isobaths.